AD-A008 554

STAR TRACKER/MAPPER: SYSTEM DESIGN PARAMETERS

F. W. Schenkel

Johns Hopkins University

Prepared for:

Naval Plant Representative Office

September 1974

DISTRIBUTED BY:

NTIS

National Technical Information Service
U. S. DEPARTMENT OF COMMERCE

Unclassified

SECURITY CLASSIFICATION OF THIS PAGE

PLEASE FOLD BACK IF NOT NEEDED FOR BIBLIOGRAPHIC PURPOSES

REPORT DOCUMENTATION PAGE

1. REPORT NUMBER APL/JHU TG 1256	2. GOVT ACCESSION NO.	3. RECIPIENT'S CATALOG NUMBER AD-A008 554
4. TITLE (and Subtitle) Star Tracker/Mapper: System Design Parameters		5. TYPE OF REPORT & PERIOD COVERED Technical Report 6. PERFORMING ORG. REPORT NUMBER
7. AUTHOR(s) F. W. Schenkel		8. CONTRACT OR GRANT NUMBER(s) N00017-72-C-4401
9. PERFORMING ORGANIZATION NAME & ADDRESS The Johns Hopkins University Applied Physics Laboratory 8621 Georgia Avenue Silver Spring, Maryland 20910		10. PROGRAM ELEMENT, PROJECT, TASK AREA & WORK UNIT NUMBERS ID 30
11. CONTROLLING OFFICE NAME & ADDRESS Naval Plant Representative's Office 8621 Georgia Ave. Silver Spring, Md. 20910		12. REPORT DATE September 1974 13. NUMBER OF PAGES 68
14. MONITORING AGENCY NAME & ADDRESS Naval Plant Representative's Office 8621 Georgia Ave. Silver Spring, Md. 20910		15. SECURITY CLASS. (of this report) Unclassified 15a. DECLASSIFICATION/DOWNGRADING SCHEDULE NA
16. DISTRIBUTION STATEMENT (of this Report) Approved for public release; distribution unlimited.		
17. DISTRIBUTION STATEMENT (of the abstract entered in Block 20, if different from Report) NA		
18. SUPPLEMENTARY NOTES NA		

Reproduced by
NATIONAL TECHNICAL INFORMATION SERVICE
US Department of Commerce
Springfield, VA. 22151

19. KEY WORDS (Continue on reverse side if necessary and identify by block number)

Design parameters
Optical sensors
Optical trackers
Spectral characteristics
Star tracker/mapper

20. ABSTRACT (Continue on reverse side if necessary and identify by block number)

This document treats a variety of topics which must be considered by the designer of a star sensor system. The intent of the document is to consolidate these factors and relate their interdependence to provide an orderly design procedure. An attempt is made to relate the star sensor design to its specific application, whether satellite or earth-based. Among the topics discussed are general systems considerations, star characteristics, atmospheric effects, optics and photometry, and available sensor types. The prospective designer is alerted to avoid the many pitfalls which he might encounter. Specific systems concepts are not discussed since the referenced literature serves to accomplish this in an adequate manner.

DD FORM 1 JAN 73 1473

PRICES SUBJECT TO CHANGE

Unclassified

SECURITY CLASSIFICATION OF THIS PAGE

APL/JHU
TG 1256
SEPTEMBER 1974

Technical Memorandum

STAR TRACKER/MAPPER: SYSTEM DESIGN PARAMETERS

by F. W. SCHENKEL

THE JOHNS HOPKINS UNIVERSITY • APPLIED PHYSICS LABORATORY
8621 Georgia Avenue ◦ Silver Spring, Maryland ◦ 20910
Operating under Contract N00017-72-C-4401 with the Department of the Navy

Approved for public release; distribution unlimited.

SUMMARY

This document treats a variety of topics which must be considered by the designer of a star sensor system. The intent of the document is to consolidate these factors and relate their interdependence to provide an orderly design procedure. An attempt is made to relate the star sensor design to its specific application, whether satellite or earth-based. Among the topics discussed are general systems considerations, star characteristics, atmospheric effects, optics and photometry, and available sensor types. The prospective designer is alerted to avoid the many pitfalls which he might encounter. Specific systems concepts are not discussed since the referenced literature serves to accomplish this in an adequate manner.

Preceding page blank

ACKNOWLEDGMENT

This document offers a compendium of information distilled from many sources, particularly those listed in Section 7, and from the writer's own experience.

The author also wishes to acknowledge the many helpful suggestions made by Dr. Joseph Bucciero, CLR, while editing the text.

Preceding page blank

CONTENTS

List of Illustrations 9
List of Tables 11
1. General System Considerations. 13
2. Stars 17
Spectral Types 17
Magnitude Scales 24
3. Earth-based versus Space-based Systems . . 31
Atmospheric Effects 32
Background Effects 36
4. Optics and Photometry 39
The Optical System 39
Photometry 41
Spectral Properties 43
5. Star Sensor Detectors 47
Photomultipliers 47
Image Dissectors 50
Vidicon 54
Image Orthicon. 57
See Saw Image Correlation Tubes. . . . 59
6. Star Sensor Systems 65
7. References 67

Preceding page blank

ILLUSTRATIONS

1.	Functional Block Diagram of Star Tracker/ Mapper	14
2.	Diagram of Satellite-Earth Orientation	15
3.	Celestial Sphere and Equatorial Coordinates	18
4.	Navigational Star Chart	19
5.	Black-body Radiation Curves for Various Temperatures	20
6.	Stellar Background Based on Color Temperature and Type Distribution	22
7.	Stellar Background Based on Effective Temperature and Type Distribution	23
8.	Hertzsprung-Russell Diagram	25
9.	Hertzsprung-Russell Diagram for the Brightest Stars	29
10.	Power Density versus Visual Magnitude of Celestial Bodies	30
11.	Atmospheric Transmission through One Air Mass	33
12.	Relationship between the Resolving Power of an Objective and the Aperture Diameter for Various Star Energy Percentages	42
13.	Power Available in Visible Region for a Given Magnitude Star as a Function of Objective Diameter	44
14.	Spectral Response of Photoemissive Surfaces	48
15.	Various Dynode Configurations in General Use	49
16.	Image Dissector Schematic Representation	50

Preceding page blank

ILLUSTRATIONS (cont'd)

17. Vidicon Schematic Representation . . 54

18. Image Orthicon Schematic Representation . 57

19. Signal Correlation of Two Images . . 60

20. Type F4067 Schematic 61

21. Correlation Tubes Outline Drawings . 63

22. The Relation between False Alarm Probability and Signal-to-Noise Ratio . 66

TABLES

1. Star Type Effective Temperature and Bolometric Correction 27

2. The 25 Brightest Stars 28

3. Refraction Corrections for Zenith Angles at Sea Level 34

4. Refraction Corrections, Scaled for Altitude of Observer 35

5. Sources Contributing to Night Sky Illuminance 37

6. Night Sky Radiance 37

7. Factors Influencing Image Frame Time . 65

1. GENERAL SYSTEMS CONSIDERATIONS

Star sensors fall into two general categories, i.e., trackers and mappers. A star tracker is a sensing system which detects, locks onto and follows a specific star. A star mapper does not lock onto a specific star but obtains a picture of a section of the heavens or celestial sphere. A star tracker is most often used in a closed loop system. Star mappers most often are operated open loop where only the measure of a particular position rather than its control is desired. The star tracker or mapper may be either gimbal mounted or strapped-down. This is very much mission dependent. For example, satellite applications usually employ a strap-down mounting. An earth-based application such as a shipboard or aircraft installation most often would utilize a gimbal mounting.

The actual star sensing element can be any of a number of devices, but most frequently photomultiplier tubes, image dissectors, image orthicons and a variety of vidicons. Once again the detector type which one selects is very much mission dependent. For example, a photomultiplier type star sensor, whether it is used as a tracker or a mapper, would not be a good candidate for a three-axis gradient satellite. Such a mission requires a star sensor which has some inherent scan capability. Since electronic scan is preferred over a mechanical mirror scan system, a TV camera tube type sensor becomes more desirable. If on the other hand one is dealing with a spin stabilized satellite, a photomultiplier sensor makes good sense. The photomultiplier requires much less sophisticated electronics than does a camera tube.

In space applications it is always a good policy to maintain maximum simplicity commensurate with the mission requirements and the operational parameters imposed by the spacecraft.

Preceding page blank

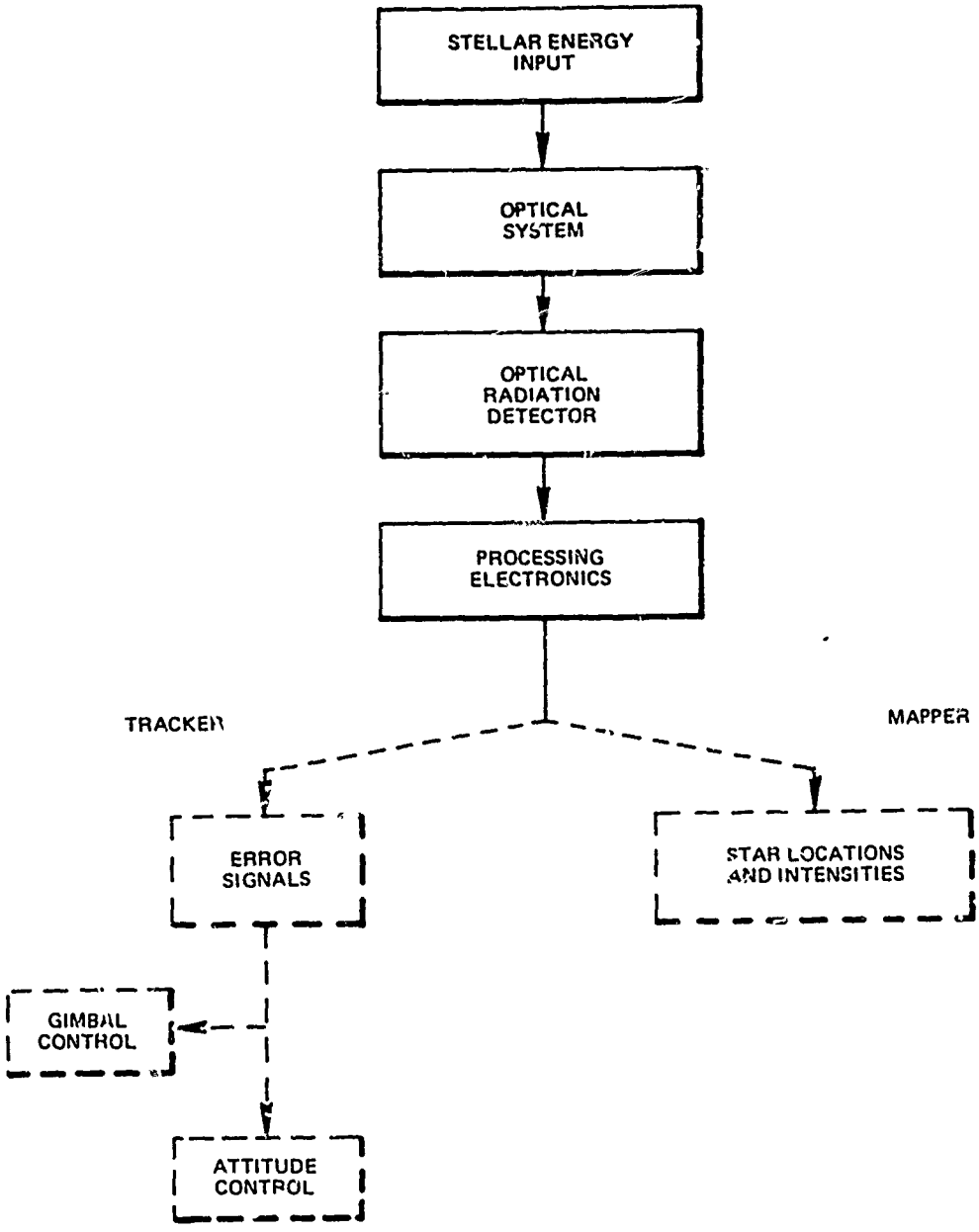

Fig. 1 FUNCTIONAL BLOCK DIAGRAM OF STAR TRACKER/MAPPER

Figure 1 is a functional block diagram of a star tracker/mapper. Figure 2 is a diagram showing a typical satellite-Earth orientation.

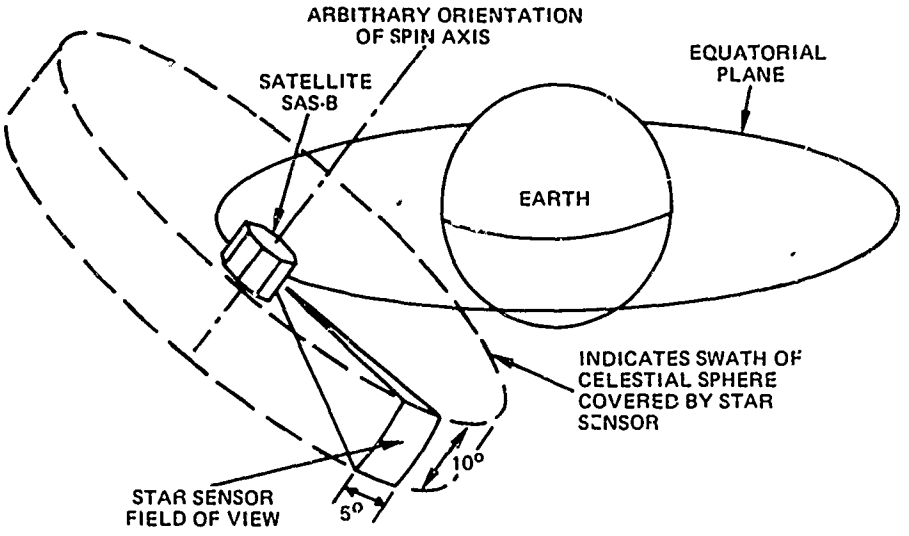

Fig. 2 DIAGRAM OF SATELLITE-EARTH ORIENTATION

2. STARS

Stars are conventionally catalogued and charted in terms of the familiar astronomical coordinates system which uses the equator as a base plane. In a geocentric system Right Ascension is measured eastward from the vernal equinox along the celestial equator to the hour circle of the star, and is expressed in hours (or in degrees). Declination is positive or negative (North or South) and is measured in degrees from the celestial equator along the hour circle to the star. Figure 3 illustrates the geometry of this system. Figure 4 is a navigational star chart in equatorial geocentric coordinates.

Stars are divided into spectral classes and magnitudes according to their spectral radiation and the intensity of the received radiation.

SPECTRAL TYPES

The spectral distribution is used to assign to a star a temperature based on fitting a blackbody radiation curve to the measured spectrum. There are two primary temperature scales. The first scale gives the color temperature of the stars, and is defined as the temperature of a blackbody radiating with the same spectral distribution within the visible region as that observed from the star. The second scale gives the effective temperature of the stars, and is defined as the temperature of a blackbody radiating with nearly the same spectral distribution over the entire spectrum as that observed from the star. Figure 5 shows the blackbody radiation curves for various temperatures.

Preceding page blank

A. CELESTIAL EQUATOR
B. ECLIPTIC (APPARENT PATH OF THE SUN)
C. VERNAL EQUINOX
D. CELESTIAL BODY
E. EARTH
F. HOUR CIRCLE OF CELESTIAL BODY
G. ZERO HOUR CIRCLE
C–H. RIGHT ASCENSION
H–D. DECLINATION
E–D. GEOCENTRIC RADIUS VECTOR

NCP – NORTH CELESTIAL POLE
SCP – SOUTH CELESTIAL POLE

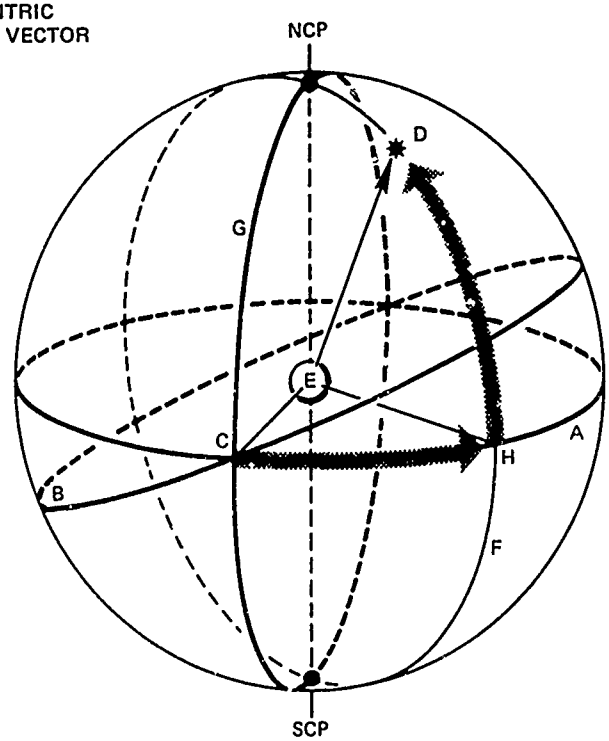

Fig. 3 CELESTIAL SPHERE AND EQUATORIAL COORDINATES

THE JOHNS HOPKINS UNIVERSITY
APPLIED PHYSICS LABORATORY
SILVER SPRING, MARYLAND

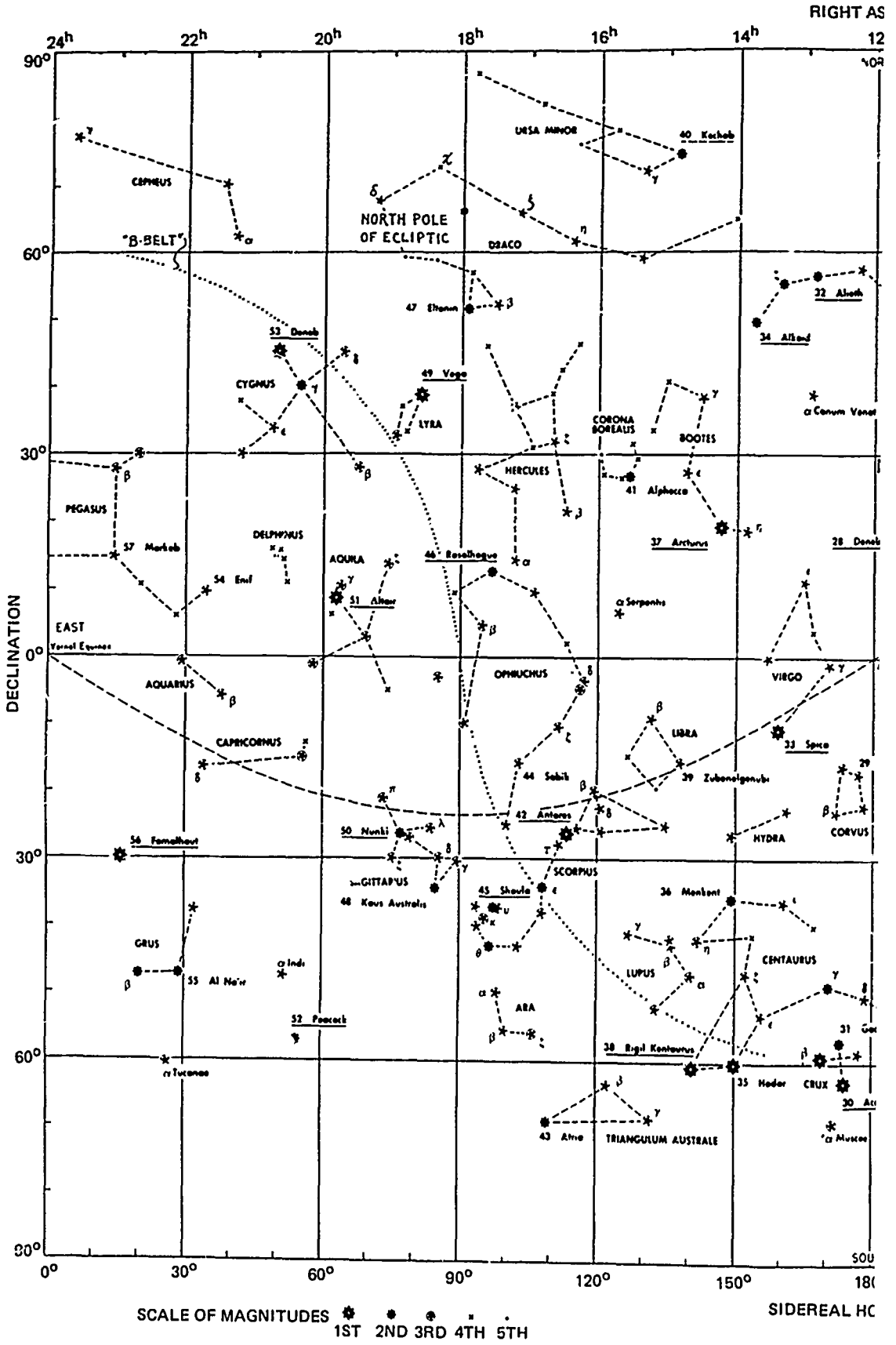

A

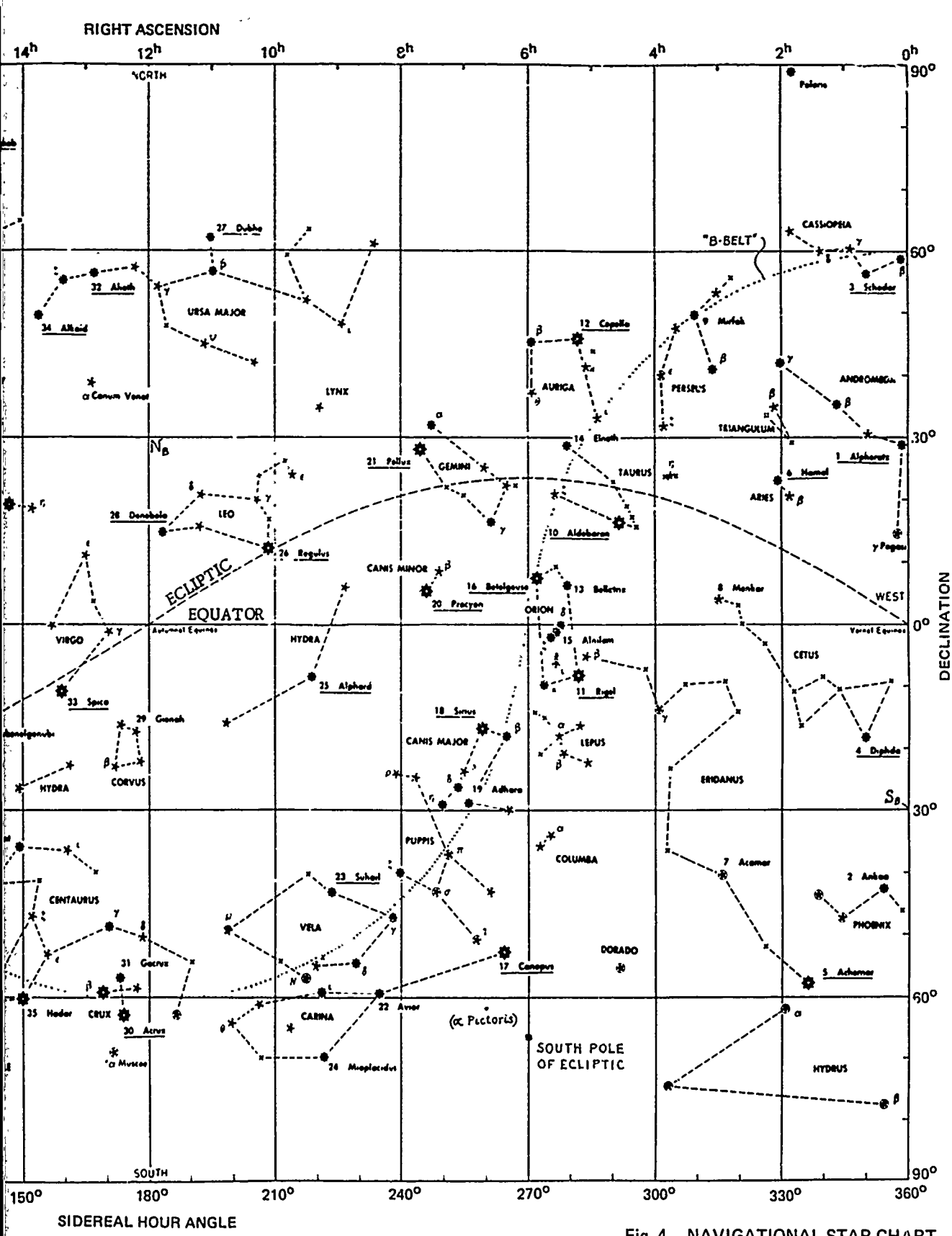

Fig. 4 NAVIGATIONAL STAR CHART

B

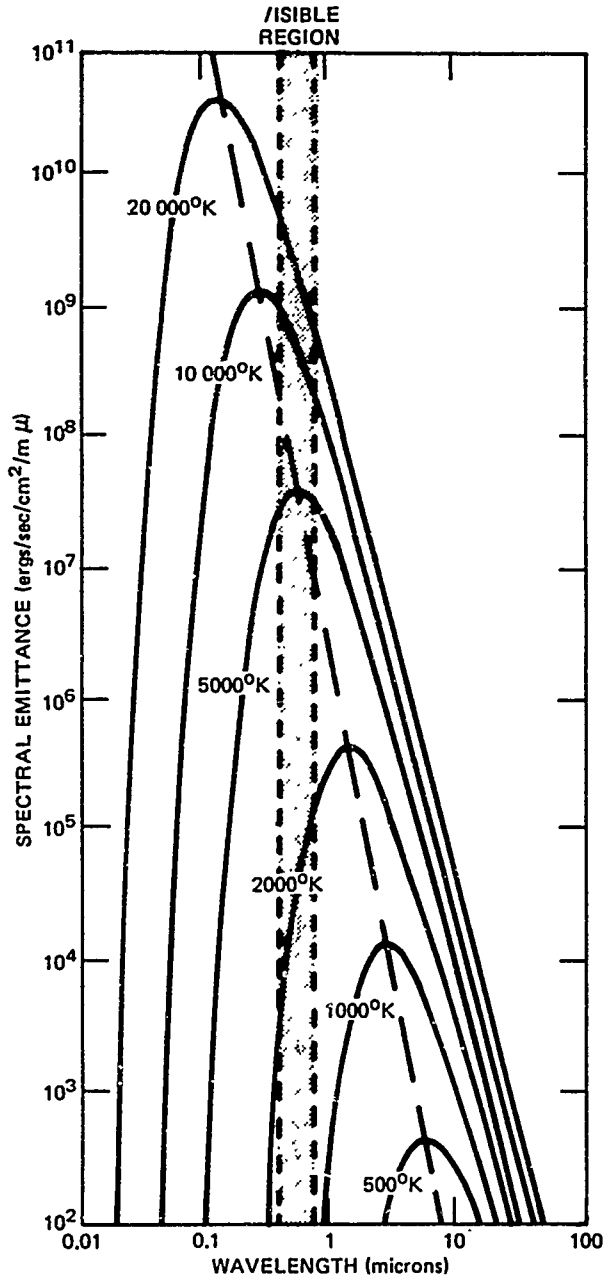

Fig. 5 BLACK-BODY RADIATION CURVES FOR VARIOUS TEMPERATURES

The visual color temperature for the main sequence stars and the theoretical wavelength of maximum radiation are:

Type	Color Temperature (degrees K)	Calculated Wavelength of Maximum Radiation (microns)
B0	38 000	0.076
A0	15 400	0.170
F0	9 000	0.320
G0	6 700	0.432
K0	5 400	0.545
M0	3 800	0.765

The effective temperatures are based on the total radiant flux and result in a cooler temperature because a star is not a classic radiator especially at the shorter wavelengths.

Type	Effective Temperature (degrees K)	Calculated Wavelength of Maximum Radiation (microns)
B0	22 000	0.132
A0	10 700	0.271
F0	7 400	0.393
G0	5 900	0.491
K0	4 900	0.592
M0	3 600	0.805

Figure 6 illustrates stellar type spectral distribution based upon color temperature. Figure 7 illustrates stellar type spectral distribution based upon effective temperature.

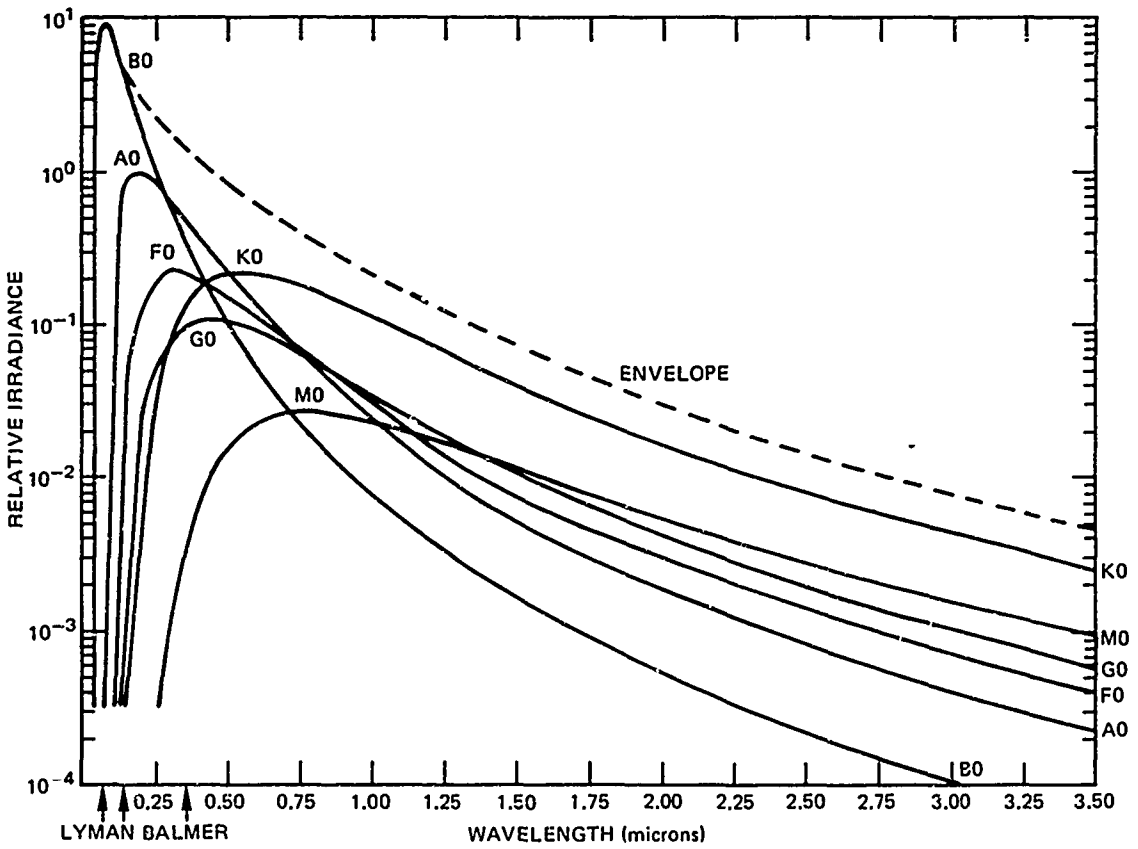

Fig. 6 STELLAR BACKGROUND BASED ON COLOR TEMPERATURE AND TYPE DISTRIBUTION

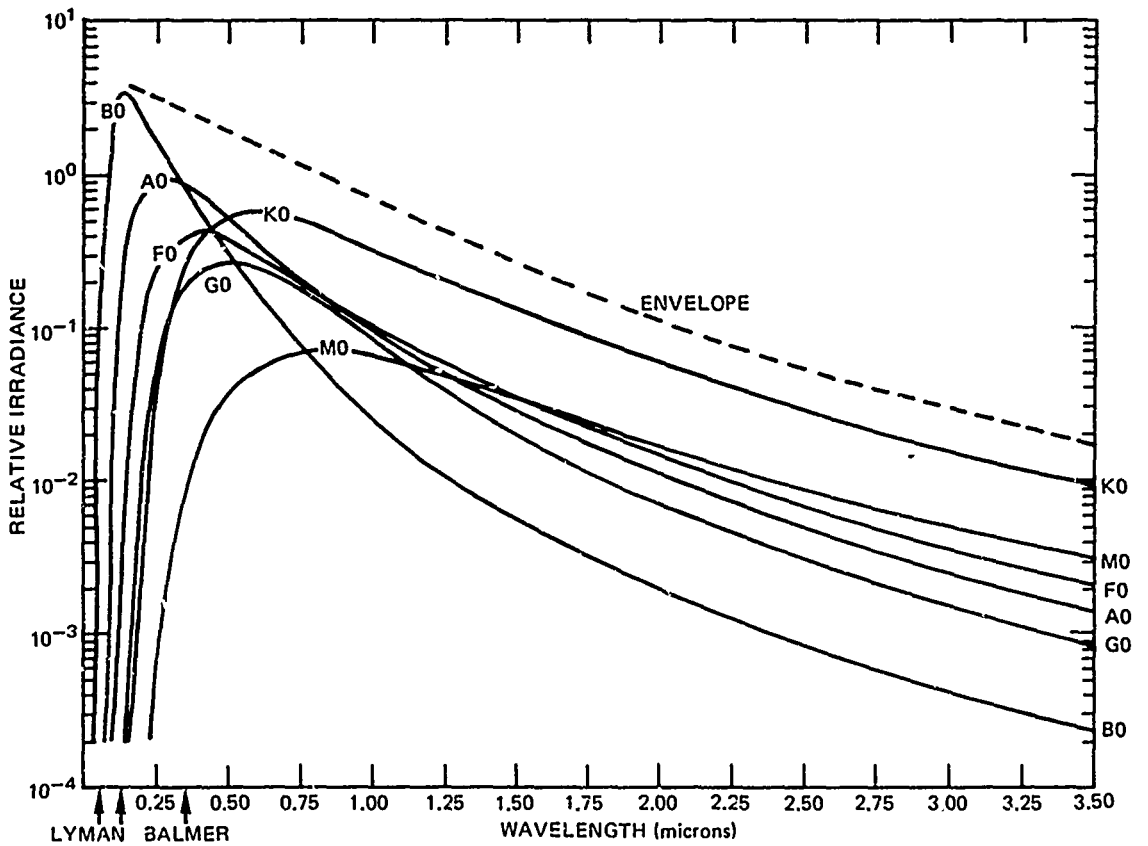

Fig. 7 STELLAR BACKGROUND BASED ON EFFECTIVE TEMPERATURE AND TYPE DISTRIBUTION

Figure 8 shows the Hertzsprung-Russell diagram. It is to be noted that 99% of the known stars are contained within the six letter classification shown for the main sequence stars. Each class is further divided into 10 subdivisions, from 0 to 9 in order of decreasing temperature. Shown on the same diagram is the relative luminosity of the stars in terms of the Sun.

The full spectral class designation of a normal star consists of three items: an upper case letter and an arabic numeral to denote the temperature class, and a roman numeral to denote the luminosity class. For example, αCMa (Sirius) is A1V. In addition to the standard spectral notation, lower case letters may be added to show certain nonstandard features in the spectrum (see Fig. 8).

Astronomers also categorize stars by a wideband UBV photometric system. The designations U, B and V each represent a filter with a given spectral distribution as sensed with a photomultiplier tube having an S4 (blue-sensitive) spectral characteristic. The ratio of any two of these filtered outputs from a particular star is representative of a given color temperature. This photometric system is not particularly useful for star tracker/mapper design.

MAGNITUDE SCALES

Several magnitude scales are used in astronomy. The brightness to magnitude conversion is constant for all systems, but the spectral response of the detectors is different. Some detectors are more sensitive to the blue colors and see blue stars as the brighter stars; conversely, red-sensitive detectors detect more of the energy of the cooler red stars. The common reporting scales are the photographic and the photovisual; the reported magnitudes, photographic and photovisual, are indicated with the symbols m_{pg} and m_{pv} respectively. The photovisual and standard eye scales are often used interchangeably although they do not exactly match. Two additional magnitude scales are the

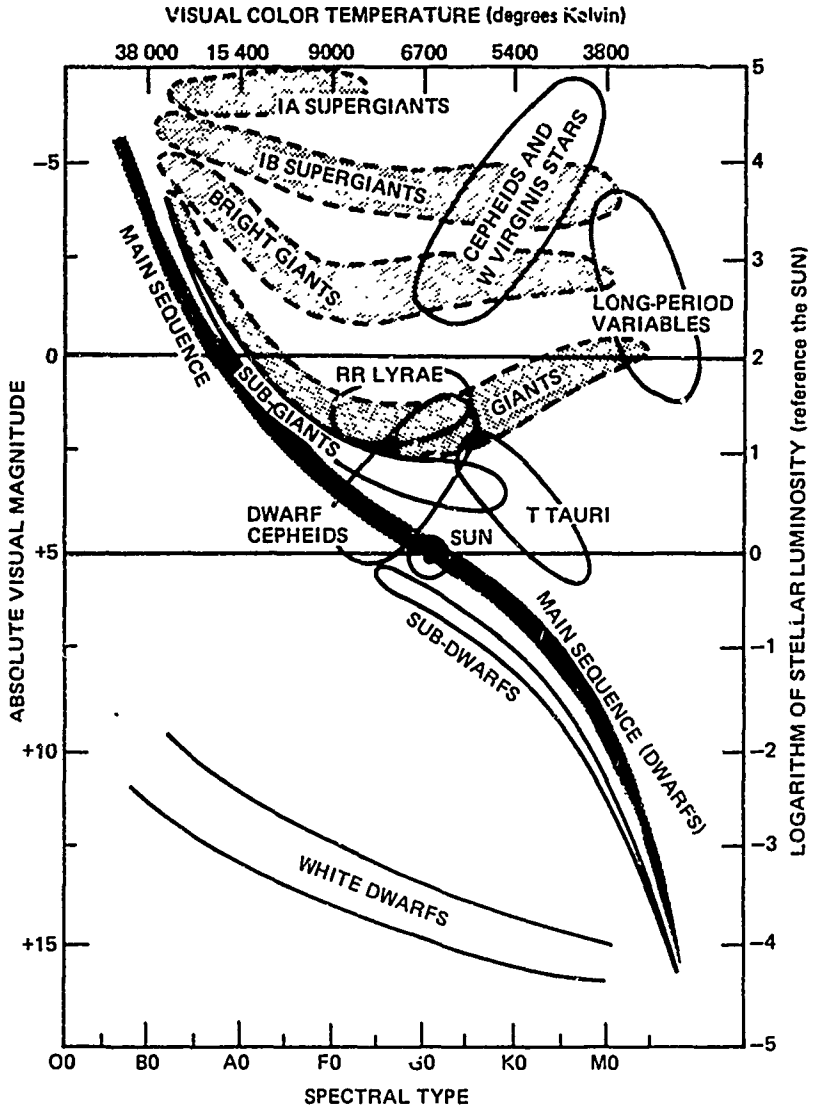

LUMINOSITY CLASS (widely used)

Supergiants:	
most luminous	Ia
less luminous	Ib
Bright Giants	II
Normal Giants	III
Sub-giants	IV
Main Sequence	V

TEMPERATURE CLASS SUFFIXES

e = Emission lines
k = Interstellar lines
m = Metallic lines
n = Nebulous (broad) lines
p = Peculiar spectrum
s = Sharp lines
v = Variable

Fig. 8 HERTZSPRUNG–RUSSEL DIAGRAM

bolometric (m_{bol}) and the radiometric (m_{rad}). The bolometric magnitude scale is based on the total radiation from the star — ultraviolet, light, radio, heat, etc. — irrespective of wavelength. The radiometric scale is based on the total radiation received through one air mass, i.e., at the zenith.

The conversions from one scale to the other are defined as follows:

$$m_{pv} - m_{bol} = \text{BC (bolometric correction)}$$

$$m_{pv} - m_{rad} = \text{HI (heat index)}$$

$$m_{pg} - m_{pv} = \text{CI (color index)}$$

The standard bolometric irradiance is 2.27×10^{-12} watts/cm^2 and this defines the zero bolometric star. The effective temperature describes a smoothed spectral distribution of the star irradiance.

A short table containing the bolometric corrections for the main sequence stars is shown in Table 1.

Absolute magnitude of a star is a measure of stellar lumininosity and is defined as the apparent magnitude of a star if it were placed at the standard distance of 10 parsecs (32.6 light years). Photographic and visual absolute magnitudes are symbolized respectively by M_p and M_v.

Table 2 gives a listing of the visual magnitudes of the 25 brightest star. Figure 9 presents the Hertzsprung-Russell diagram for the same celestial bodies. Figure 10 illustrates the relationship between stellar radiant flux (watts/cm^2) and apparent visual magnitude in addition to defining the stellar distribution as a function of magnitude.

Table 1

Star Type Effective Temperature
and Bolometric Correction

Type	Effective Temperature	Bolometric Correction
O5	35 000°K	5.0
B0	22 000°K	2.9
B5	14 000°K	1.4
A0	10 700°K	0.60
A5	8 500°K	0.20
F0	7 400°K	0.00
F5	6 500°K	0.00
G0	5 900°K	0.05
G5	5 500°K	0.10
K0	4 900°K	0.17
K5	4 200°K	0.6
M0	3 600°K	1.2
M5	2 800°K	2.4

Table 2

The 25 Brightest Stars

Celestial Body	Proper Name	Apparent Magnitude m_v	Spectral Type	Absolute Magnitude M_v
αCMa	Sirius	-1.47	A1 V	+0.7
αCar	Canopus	-0.71	F0 Ib	-5.5
αCen	Rigil Kent	-0.27	G2 V	+4.6
αBoo	Arcturus	-0.06	K2 IIIp	-0.3
αLyr	Vega	+0.03	A0 V	+0.3
βOri	Rigel	0.08	B8 Ia	-7.0
αAur	Capella*	0.09	G8 III G0 III	+0.12 +0.37
αCMi	Procyon	0.34	F5 IV-V	+2.8
αEri	Achernar	0.49	B5 V	-1.3
βCen	Hadar	0.61	B1 III	-4.3
αAql	Altair	0.75	A7 IV-V	+2.1
αTau	Aldebaran	0.78	K5 III	-0.2
αCru	Acrux	0.80	B1 IV	-3.8
αOri	Betelgeuse†	0.85‡	M2 Ib	-5.5
αSco	Antares	0.92	M1 Ib	-4.5
αVir	Spica	0.98	B1 V	-3.2
βGem	Pollux	1.15	K0 III	+0.7
αPsA	Fomalhaut	1.16	A3 V	+1.8
αCyg	Deneb	1.26	A2 Ia	-7.0
βCru	Mimosa	1.28	B0 IV	-4.0
αLeo	Regulus	1.33	B7 V	-1.0
εCMa	Adhara	1.42	B2 II	-5.0
γOri	Bellatrix	1.61	B2 III	-4.1
λSco	Shaula	1.61	B2 IV	-3.3
βTau	El Nath	1.64	B7 III	-3.0

*Binary
†Variable
‡Mean

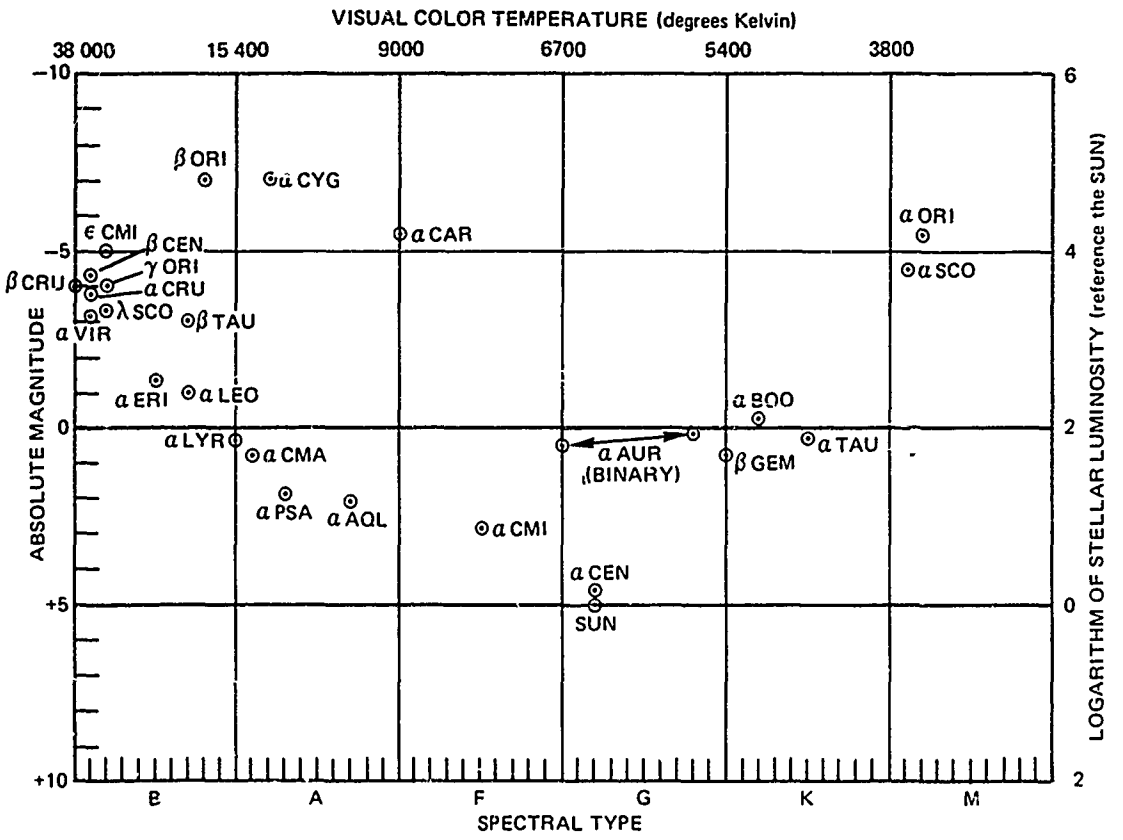

Fig. 9 HERTZSPRUNG–RUSSELL DIAGRAM FOR THE BRIGHTEST STARS

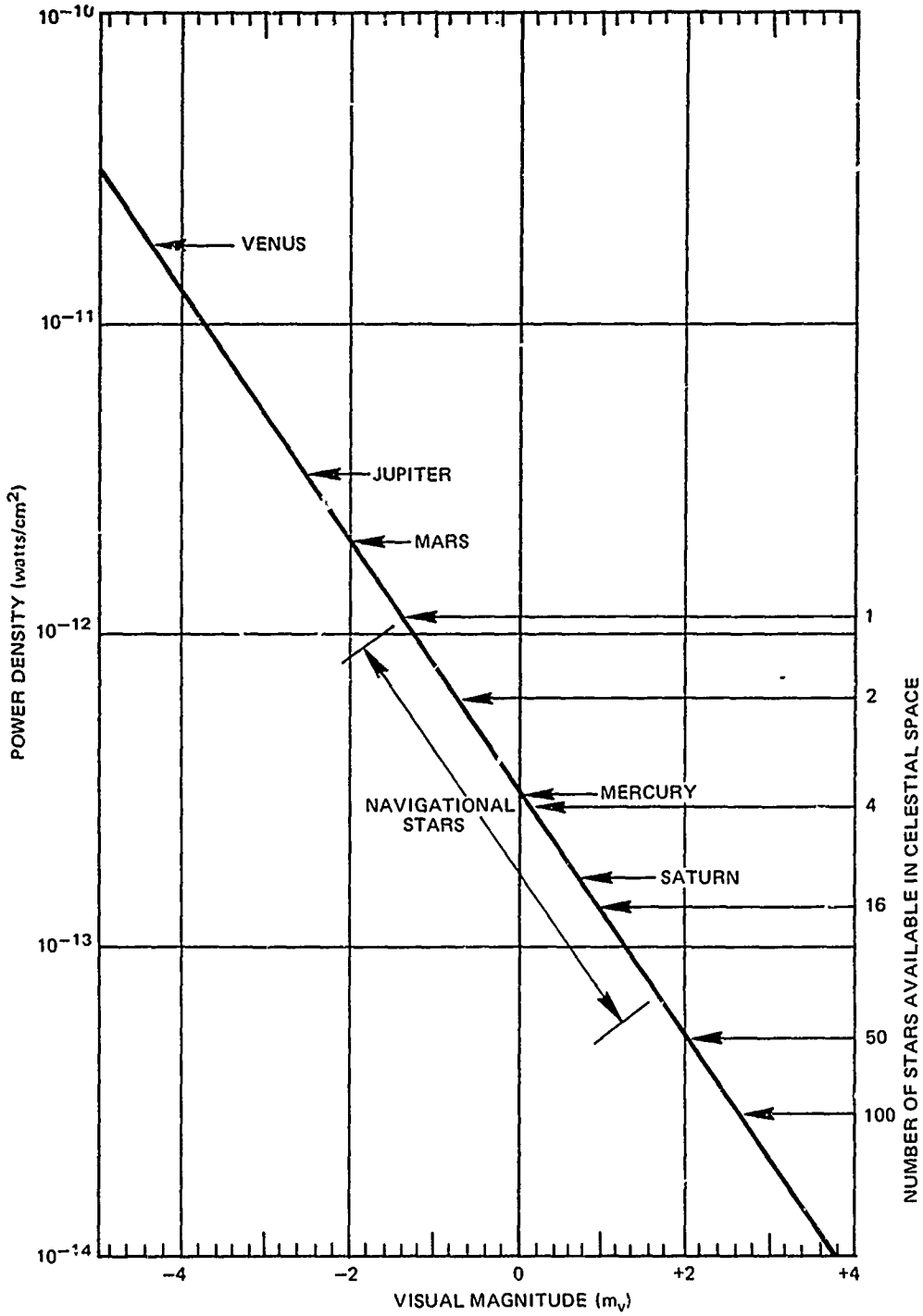

Fig. 10 POWER DENSITY VERSUS VISUAL MAGNITUDE OF CELESTIAL BODIES

3. EARTH-BASED VERSUS SPACE-BASED SYSTEMS

Earth-based systems usually have no severe limitations placed upon weight, volume, magnetic moment, component motion, etc. In space applications weight, volume, power consumption, etc. are always of great importance. The use of magnetic materials is usually discouraged to the limit of possibly 100 pole · cm magnetic moment. The use of moving components is avoided wherever possible to prevent the introduction of mechanical moments or the need for compensating systems.

An additional factor to be considered in spaceborne systems is the influence of the radiation particle environment. For a synchronous altitude of some 23 000 miles, the following environment may be encountered:

Particle	Particle Energy (eV)	Three-year Time Integrated Integral Flux (Particles/cm^2)
Electrons	1.6×10^6	3×10^{10}
	4×10^4	3×10^{15}
Protons	3×10^7	3×10^8
	0.1×10^6 to 5×10^6	3×10^{15}

The above particles will be due to the outer Van Allen Belt.

The proton flux due to solar flares is estimated to be as follows:

Protons of 1.2×10^7 eV energy at 2×10^{12} protons/cm^2.

The tracker will be capable of survival in this type environment provided a high-purity fused silica is used as a lens glass or as a protective cover plate over standard optical materials.

ATMOSPHERIC EFFECTS

Attenuation

In spaceborne applications of star sensors, the designer is not particularly concerned about the effects of atmospheric attenuation. However, in earth-bound star sensing, the atmospheric attenuation can be quite significant and limiting. Figure 11 illustrates the effect of one air mass, i. e., looking to the zenith, as a function of wavelength in the visible region.

Refraction

Refraction of light is the change in the direction of a light ray as it passes from one medium to another. The change is in the direction of the normal to the interface when the ray enters a denser medium. Since the density of the atmosphere decreases with altitude, a star will appear closer to the zenith than to its actual position. Localized density anomalies, moving with the low-altitude winds, cause the apparent position of a star to move through small angles around a median position. In a photograph, a star image appears as a disc due to the random image motion. The brightness of the image also fluctuates over short time intervals. The brightness fluctuations appear to be produced by density anomalies moving with the high-altitude winds.

Table 3 gives a listing of the refractive corrections for zenith angles at sea level. Table 4 shows refraction corrections scaled for altitude.

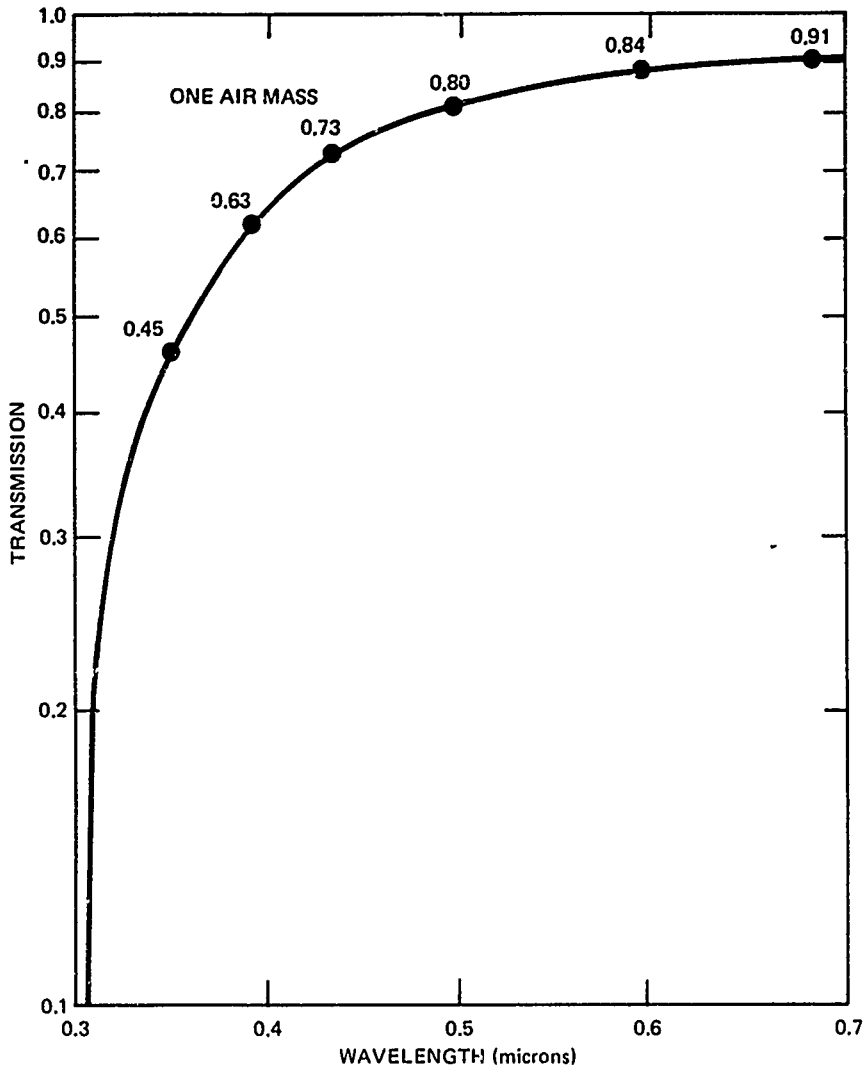

Fig. 11 ATMOSPHERIC TRANSMISSION THROUGH ONE AIR MASS

Table 3

Refraction Corrections for Zenith Angles at Sea Level

Apparent Zenith Angle	True Zenith Angle		
Degrees	Degrees	Minutes	Seconds
90	90	35	21
85	85	9	51
80	80	5	18
75	75	3	34
70	70	2	38
65	65	2	4
60	60	1	41
50	50	1	10
40	40	0	49
30	30	0	34
20	20	0	21
10	10	0	10
0	0	0	0

Table 4

Refraction Corrections, Scaled for Altitude of Observer

Altitude (Km)	Pressure (mm Hg)	Temperature (°C)	Refraction Scaling Ratio
0	760.0	+15	1.000
5	405.0	-18	0.589
10	197.0	-50	0.330
15	90.7	-59	0.172
20	42.0	-59	0.084
30	9.0	-48	0.041

Scintillation

The rapid changes in intensity that are independent of image motion or size are called scintillation. The atmospheric effects responsible for scintillation occur above the troposphere and are diffraction effects. The amplitude of the scintillation is inversely proportional to the telescope aperture. The image of a planet disc does not scintillate as rapidly or as noticeably as a star image because the scintillation of one part of the disc is out of phase with the scintillation of another part having a slightly different air path.

The amplitude of the scintillation increases with an increase in zenith angle. From zenith angles of 0° to 80° of arc, the scintillation amplitude is proportional to the secant of the angle, i.e., to the air mass. The resulting variation from the average brightness may be more than 35% for apertures less than five inches. The frequency of the scintillation decreases with an increase in zenith angle. Near the vertical (≈0° zenith angle), alternate bands of light and shade can produce scintillation frequencies as high as 1000 Hz. Near the horizon (≈90° zenith angle), the scintillation frequency can be as low as 5 to 10 Hz.

Shimmer

Shimmer, or image motion, is the random high frequency displacement of an image around the mean position. The instantaneous position may differ from the mean position by as much as 20 or 30 seconds of arc for telescope apertures less than four inches in diameter. The shimmer increases with an increase in the zenith angle, and decreases as telescope aperture increases.

BACKGROUND EFFECTS

The dominant background effects are different for spaceborne and earth-bound star sensors. In spaceborne applications, one is concerned with star background illumination such as the Milky Way, and lunar, solar and Earth glow interference. In an earth-bound application one is concerned with all of these plus the atmospheric airglow. Table 5 gives a breakdown of the sources contributing to the night sky illuminance. These sources are not uniformly distributed and may vary quite widely from the average values given. The galactic light results from the Milky Way. The zodiacal light is reflected sunlight scattered from a cloud of dust particles surrounding the sun that are confined to a region 25° to 50° wide centered in the ecliptic plane. The airglow intensity is most severe when looking near the horizon. The aurora occurring in the polar regions is brighter than the night airglow. The aurora arises from particle bombardment of the upper atmosphere and produces a spectrum that is brighter than the airglow spectrum. The aurora could interfere with the operation of a star tracker. Table 6 gives the night sky radiance as a function of visible wavelength.

Table 5

Sources Contributing to Night Sky Illuminance

Source	Percent Contribution Range
Starlight	25-30
Galactic	7-10
Zodiacal	7-15
Airglow	45-60

Table 6

Night Sky Radiance

Spectral Radiance, 10^{-10} watt cm^{-2} $sterad^{-1}$ $micron^{-1}$	Wavelength, microns
1.4	0.32
1.1	0.36
1.3	0.40
2.0	0.45
2.0	0.50
3.0	0.55
5.0	0.60
6.0	0.65

4. OPTICS AND PHOTOMETRY

THE OPTICAL SYSTEM

The purpose of the optical sub-system in a star tracker/mapper system is to collect and focus the stellar flux onto either the detector directly, or to focus the flux on a reticle or chopper located in or near the focal plane from which the flux is modulated and then transferred to the detector.

Major design considerations are:

- Aperture size
- Angular field of view
- Optical resolution
- Aberration
- Distortion
- Spectral transmission efficiency
- Compactness and weight of optical design
- Ease of fabrication and alignment
- Electro-mechanical means used for tracking/mapping

Types of Optical Systems

There are three types of optical systems employed in astronomical work: the reflecting, the refracting, and the hybrid or catadioptric (refracting-reflecting) system. The Cassegrain type telescope, which employs a convex secondary mirror on the optical axis, is a commonly used reflective system for celestial systems. Several variations of the Cassegranian system are possible, which differ considerably in their aberations for off-axis images and their ease of fabrication and alignment. Where refractive elements are added, the system becomes a hybrid.

Preceding page blank

The principal advantages of the pure reflective over the refracting system are high transmission efficiency throughout broad spectral regions, small focal ratios or F numbers yielding a more compact optical system, large aperture size with relatively small weight and volume, freedom from chromatic aberration and good imagery on the optical axis where a narrow field of view is employed.

The major disadvantages of the pure reflective over the refracting system are its inability to cover more than a small angular field of view (1° or less), high sensitivity to stray radiation and thermal effects, loss of primary mirror area caused by secondary surface blockage, and finally lack of mechanical rigidity.

The hybrid system retains many of the advantages of the reflecting system and reduces to a large extent the limitation of a narrow field of view. The addition of a corrector plate or lens in front of the primary mirror yields good resolution over moderate fields of view even with small F numbers.

Resolution

An important consideration in the selection of a suitable optical system is the optical resolution and its effect on flux density distribution in the focal plane.

The image of a point focused by a perfect lens is a minute pattern of concentric and progressively fainter rings of light surrounding a central dot, the whole structure being called the Airy disk. The Airy disk of a practical lens is small, and its linear radius in microns is given by the following formula:

$$R = 1.22\,\lambda \frac{F}{D}$$

where λ = wavelength of light, (in microns)
F = focal length of lens, in inches
D = objective aperture, in inches

Rayleigh found that two adjacent and equally bright stars can just be resolved if the image of one star falls somewhere near the innermost dark ring in the Airy disk of the other star. This distance d, in radians or in seconds of arc, is the angular resolution of the lens. A practical value of d with telescopes used for visual observation (at $\lambda \simeq 5600$ Å) is

$$d = 1.22 \left[\frac{\lambda \text{ (in Å)}}{D\text{(in cm)}} \right] \text{ radians, or } d = \left[\frac{5.5}{D\text{(in inches)}} \right] \text{ seconds of arc,}$$

where D is again the objective aperture (see Fig. 12).

However, Rayleigh criterion does not adequately describe the distribution of stellar flux in the focal plane, and therefore does not provide a complete description of the optical system resolution. Figure 12 gives the minimum angle of resolution as defined by the Rayleigh criterion and also shows the relationship between the resolving power of an objective and the aperture diameter for various star energy percentages. It is obvious from Fig. 12 that, if 95% of the stellar energy is desired for our tracking/mapping system, the angular size of the detector or of the reticle (from which the flux is modulated and then transferred to the detector) in the focal plane must be fully seven times larger than that specified by Rayleigh's criterion.

Focal length

The required optical focal length is calculated from the angle subtended by the star field of view (FOV) to be covered and the physical size of the detector element used, that is

$$\text{Optical focal length} = \frac{\text{detector size}}{2 \tan(\frac{1}{2} \text{ FOV})}.$$

PHOTOMETRY

The effective irradiance from a star as seen by a standard observer may be readily computed from the following formula:

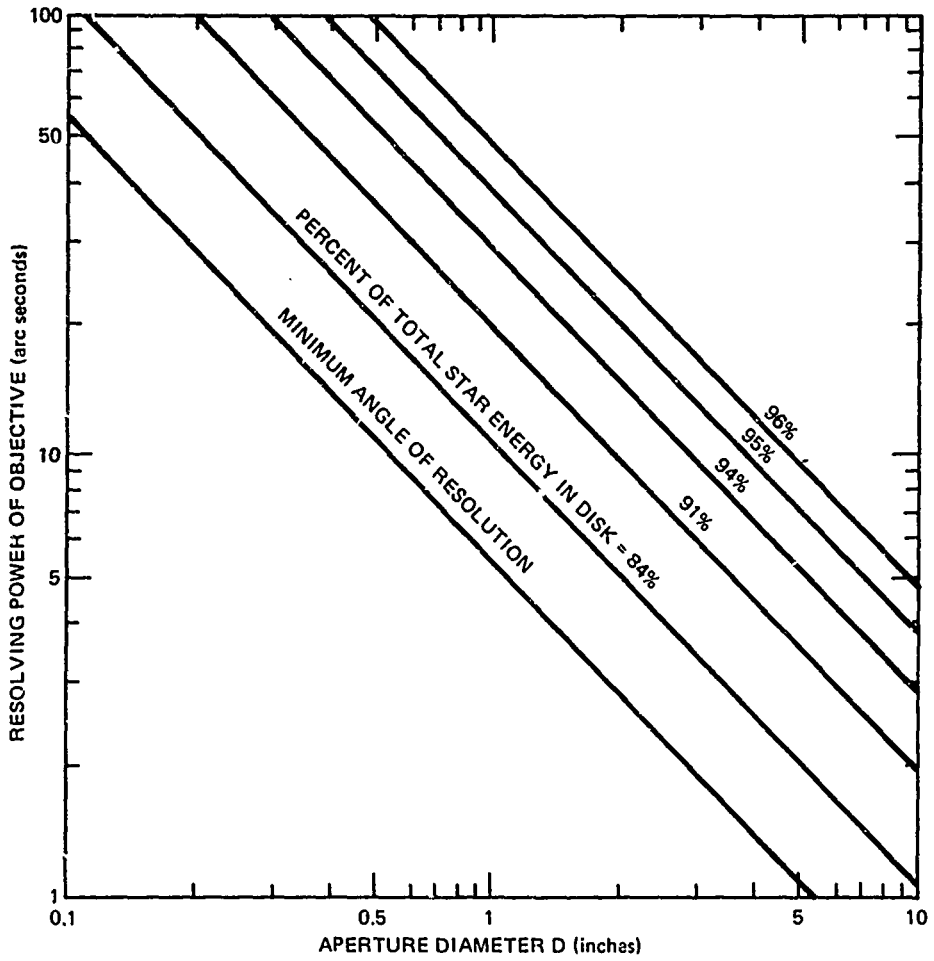

Fig. 12 RELATIONSHIP BETWEEN THE RESOLVING POWER OF AN OBJECTIVE AND THE APERTURE DIAMETER FOR VARIOUS STAR ENERGY PERCENTAGES

$$I = I_o (2.51)^{-m_v} \text{ watts/cm}^2$$

where:

I_o = watts/cm^2 for a "0" visual magnitude A0 star

$= 3.1 \times 10^{-13}$ watts/cm^2

m_v = visual magnitude.

The total available effective power P from the star that is intercepted and passed through the lens is given by

$$P = 2.43 \times 10^{-13} \beta D^2 (2.51)^{-m_v}$$

where:

β = optics efficiency

D = objective diameter, in centimeters.

Based upon the use of a 2-inch (5 cm) aperture objective with an efficiency β of 0.65 and a +4 visual magnitude A0 star, the computed value P is 9.90×10^{-14} watts.

Figure 13 gives the available stellar power intercepted by an objective of aperture D for various star visual magnitudes.

SPECTRAL PROPERTIES

Since the star sensor's spectral response does not match that of the eye, equal visual magnitude stars will not, in general, give equal outputs. It is necessary to relate the sensor's response to different spectral classes of a given visual magnitude, because stars are normally tabulated according to visual magnitude and it is convenient to be able to speak the same language.

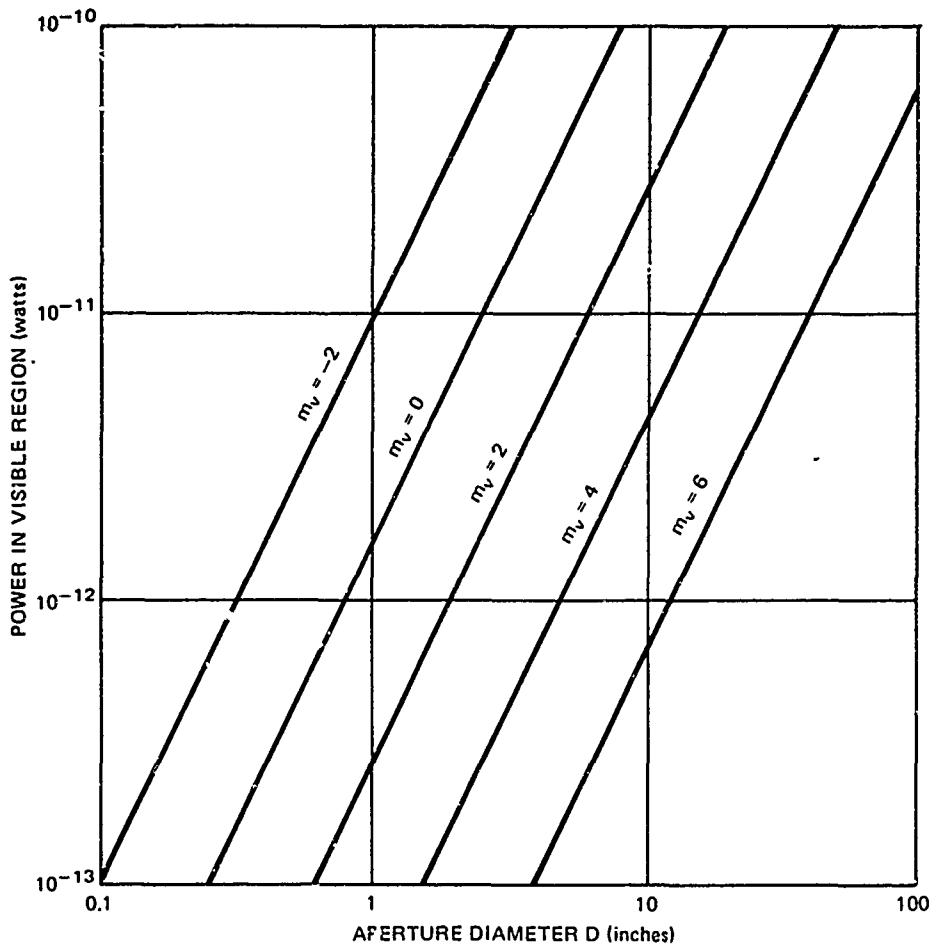

Fig. 13 POWER AVAILABLE IN VISIBLE REGION FOR A GIVEN MAGNITUDE STAR AS A FUNCTION OF OBJECTIVE DIAMETER

Because it is essential to relate the composite star mapper spectral characteristics to some measurable laboratory photometric quantities, calibration of the sensor in the laboratory is performed with a 2870°K light source, although this is significantly different from the effective temperature of the stars.

Expressed mathematically, the star sensor's spectral dependence is given by

$$X = \frac{\int_0^\infty W_2(\lambda)R_s(\lambda)d\lambda}{\int_0^\infty W_1(\lambda)R_s(\lambda)d\lambda} \cdot \frac{\int_0^\infty W_1(\lambda)R_\epsilon(\lambda)d\lambda}{\int_0^\infty W_2(\lambda)R_\epsilon(\lambda)d\lambda}$$

where:

X = relative response of star sensor to a source of spectral characteristic W_2 compared to response to a source of characteristic W_1

$W_1(\lambda)$ = power spectral density of source 1 (watts/unit wavelength)

$W_2(\lambda)$ = power spectral density of source 2 (watts/unit wavelength)

$R_s(\lambda)$ = spectral response of star sensor (amperes/watt)

$R_\epsilon(\lambda)$ = relative sensitivity of eye at wavelength λ.

By performing the indicated computations, it can be shown that the sensor's response to an A0 star relative to its response to a K0 star is 1.30. This ratio corresponds to a change in star magnitude of 0.3. Hence, given two stars of types A0 and K0 with equal visual magnitudes, the sensor's output will indicate a difference of 0.3 magnitude. Similarly, the sensor's response to a K0 source relative to a 2870°K source is computed as 0.955.

5. STAR SENSOR DETECTORS

Detectors suitable for star sensing applications are generally of the quantum type, in which either electrons are ejected by the absorbed quanta (photoemissive) or charge carriers are created within the material (photoconductive, photovoltaic).

For the most part photoemissive detectors are utilized. These include photomultipliers, image dissectors, image orthicons, image intensifiers, correlatrons and certain intensifier type vidicons. The standard vidicon utilizes a photoconductive retina. Its spectral response runs from 0.4 to 1.1 microns. Figure 14 illustrates the spectral characteristics of the photoemissive sensors most often used in star sensing applications.

PHOTOMULTIPLIERS

In a photomultiplier, photoelectrons are emitted by quanta of light impinging on the photocathode. The photoelectrons being emitted in a vacuum are electrostatically directed into a secondary multiplier which consists of a number of dynodes. Each dynode has a secondary emitting surface. Primary photoelectrons striking the first dynode cause two or more secondary electrons to be emitted for every primary electron. These secondary electrons are focused to strike the second dynode where the process is repeated. After about 10 to 14 dynodes the amplified current is collected on an anode plate or grid. The total gain may range from 10^3 to 10^7 at a bandwidth of up to 1 GHz. Figure 15 illustrates some typical photomultiplier layouts.

Preceding page blank

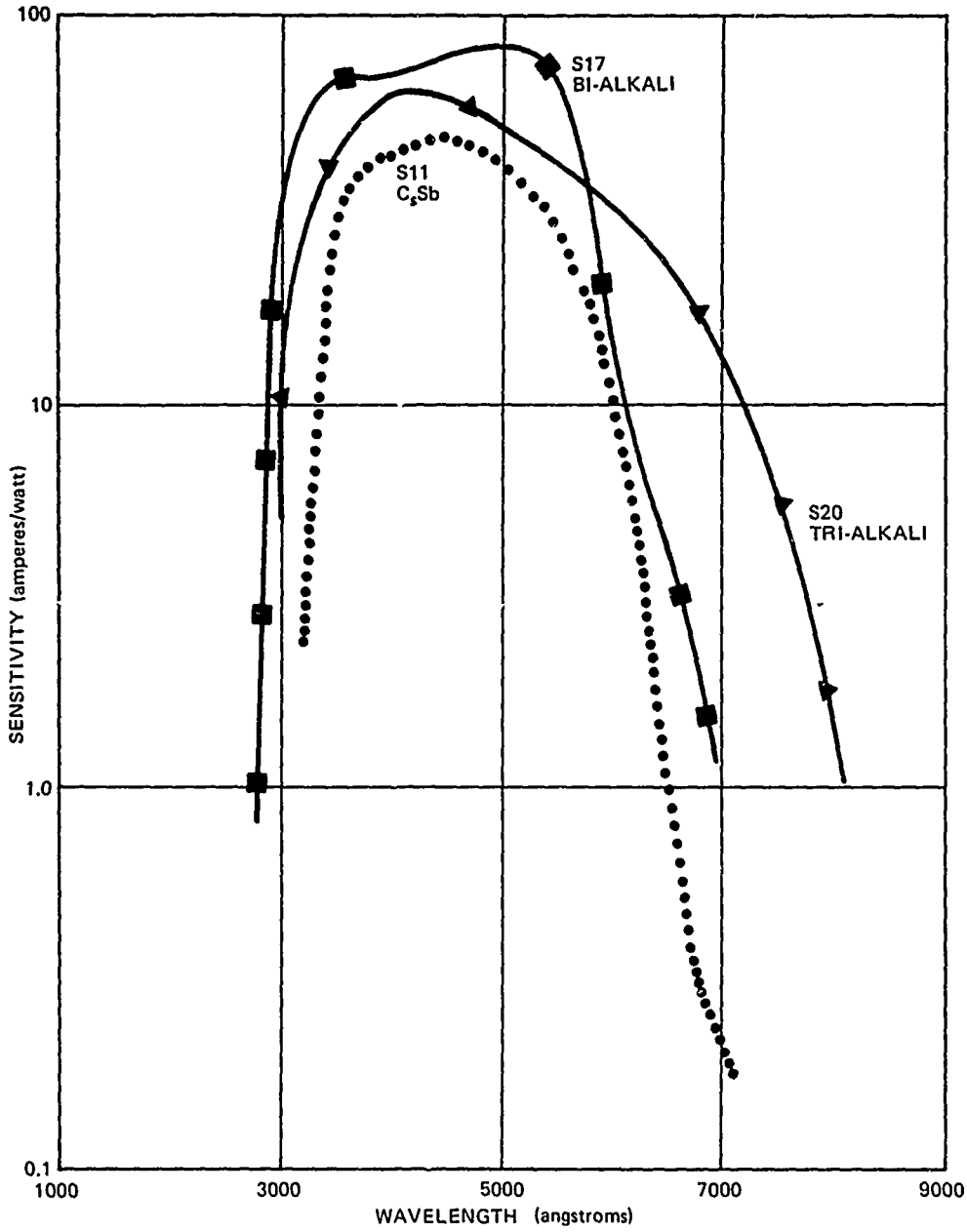

Fig. 14 SPECTRAL RESPONSE OF PHOTOEMISSIVE SURFACES

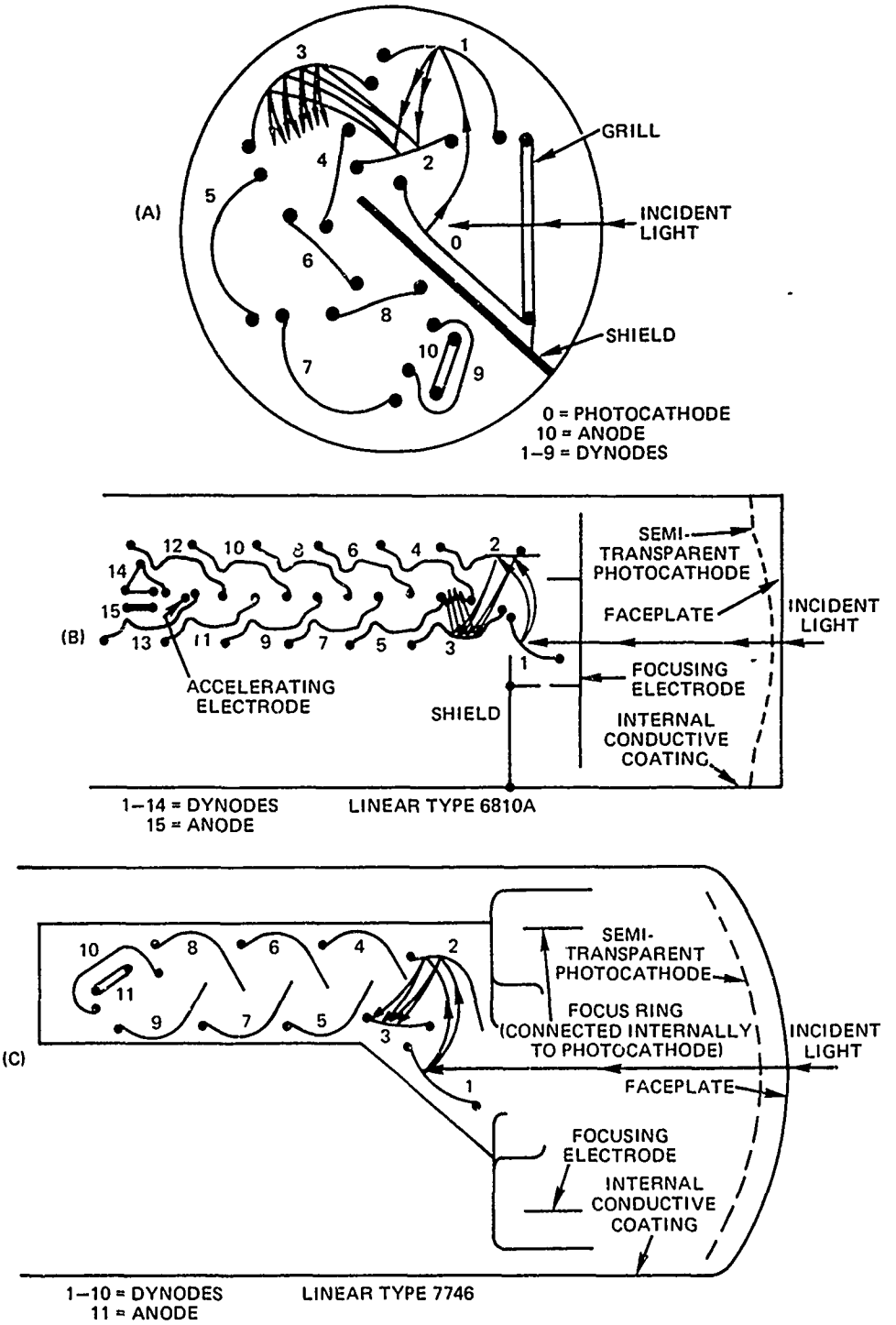

Fig. 15 VARIOUS DYNODE CONFIGURATIONS IN GENERAL USE: (A) CIRCULAR-CAGE TYPE; (B) AND (C) LINEAR TYPES

IMAGE DISSECTORS

The image dissector is a television camera tube having a continuous photocathode on which is formed a photoelectric emission pattern that is scanned by moving its electro-optical image over an aperture.

Principle of Operation

From the optical image focused on the photocathode (Fig. 16) an electro-optical image is derived that is focused in the plane containing the aperture. Two sets of scanning coils sweep this image over the aperture. At any instant, only the electrons entering the electron multiplier through the aperture are utilized. The output signal is taken from the multiplier collector.

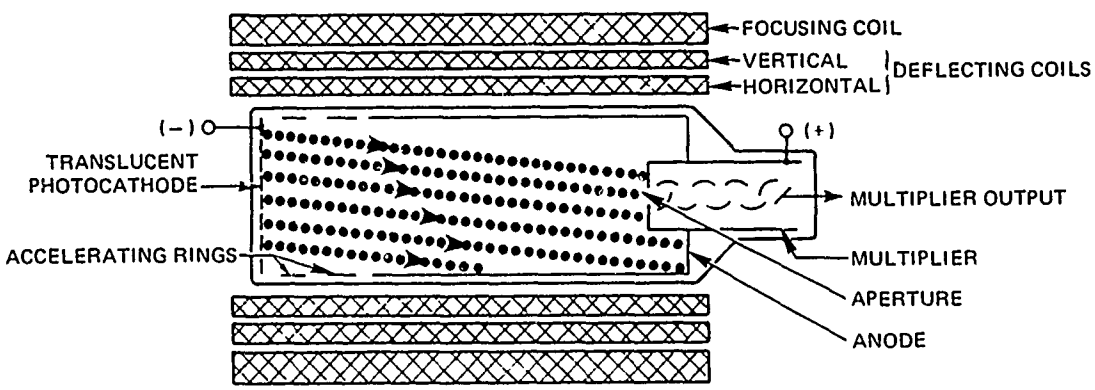

Fig. 16 IMAGE DISSECTOR SCHEMATIC REPRESENTATION

No storage means are used, and therefore, the dissector is not suitable at very-low light levels. But the output signal is proportional to the light, free from shading and, within reasonable limits, independent of temperature. The electron optics of the tube are usually designed for unity magnification. The aperture area determines the resolution.

Properties

The dissector has the following unique and rather unusual properties which should be taken into consideration when selecting an appropriate camera tube for a specific application:

- Non-Storage

Because no storage is involved, the scan rate on a dissector can be varied at will without changing the signal current amplitude. Dual or multiple scan modes can be adopted, in which an earlier large raster scan is replaced by a smaller scanned area for image analysis or image tracking.

- High Resolution

Image dissectors achieve paraxial resolutions closely predictable on the basis of selected electron beam defining aperture size. For example, in magnetically focused tubes, contrast ratios as high as 40 percent have been observed experimentally with 0.001 inch diameter apertures at 1600 TV lines / inch resolving power (800 line pairs/inch). These high resolutions are quite compatible with the ultimate limits set by the emission energies of the photoelectrons for tubes of this type, as established by G. Papp of ITTIL (IRE. Tr. on Nuclear Science, Vol. NS-9, No. 2, April 1962. p. 93).

Off-axis resolution approaching the paraxial performance can be achieved with a moderate degree of dynamic focusing only in magnetically-focused varieties. For electrostatically focused dissectors, off-axis loss of resolution, even with dynamic focusing, is appreciable.

- Linearity

The basic multiplier phototube operating principle used in image dissectors is linear over many orders of magnitude, at least 4 to 5 orders in normal usage. The

image dissector is therefore particularly useful where a wide dynamic range of signal inputs with linear response is encountered. Re-adjustment of the multiplier gain by altering the applied operating potentials can produce even greater dynamic ranges.

Response linearity from one portion of an input image to another portion of the same image is limited to some extent, as it would be in any camera tube, by internal light reflections within the camera tube envelope and variations in sensitivity of the photosensitive film. Dissectors with internal optical trapping can be supplied on special order.

- Noise

Noise in an image dissector camera normally arises from three readily identified sources: dark emission from the photocathode, background lighting on the photocathode, and the signal flux itself. The multiplier gain is normally high enough so that other noise sources, such as amplifier noise, etc., are negligible. With nearly all photocathodes except infrared sensitive types the dark emission noise is also negligible, so that the dissectors, in general, operate either under a background-noise limited or a noise-in-signal limited condition. Photon fluctuations of the flux input, modified by the quantum efficiency of the photoemissive conversion process at the photocathode, are then observable in the dissector. For location of images on a dark background, as in star tracking, the dissector may therefore be more sensitive than expected because of the almost total absence of dark noise in the nonsignal areas.

- Special Apertures

Dissectors are readily adapted to the examination of specialized portions of the input image using appropriately shaped defining apertures. Apertures can range from a long slit aperture for examining signal line scans of a spectrum to such complex apertures as pin-wheels, etc., used with special scan modes to obtain additional picture information or discriminate against certain input patterns.

- Simple Operating Theory

The operational theory of the dissector is simple and straightforward, making it possible to predict, a priori, what the resulting system capabilities will be. This is useful to the system designer and in the system check-out.

- Reliability

The dissector is a simple, rugged, reliable device without a thermionic cathode, which limits its lifetime and consumes operating power. Shelf life is many years and operating life is comparable, unless excessive input illumination occurs for long time periods. Momentary exposure to sunlight or even the sun's image does no harm.

- Fast Turn On

The dissector is ready to operate at full efficiency as fast as the associated circuitry can be activated.

- Scan Drive

The dissector is adaptable to both magnetic and electrostatic deflection, although magnetic deflection has proven to be more readily adaptable to low power transistor drive circuitry. If fast fly back or fast random access is not required, a dissector with magnetic scan can supply large amounts of picture information at high output signal levels, with a minimum of total required system power.

- Spectral Response

This includes all regions for which suitable photocathodes are available and therefore extends from the near infrared to the extreme ultraviolet region.

- Raster Edge Effects

Unlike such beam scanning tubes as the image orthicon and vidicon, the dissector has no scanned raster area

surrounded by an uncharged unscanned area. As a result no edge effects are encountered in the dissector resulting from potential discontinuities at the raster edge and showing up as abnormal signal amplitudes along all raster edges as observed in image orthicons and vidicons. A small raster of for example only 5 or 6 short scan lines can be located anywhere on the dissector sensitive area, with each scan line, even at the edges, contributing proper signal amplitudes.

VIDICON

This type of star sensor has been used on almost every satellite containing a TV camera including the DODGE satellite.

The vidicon is a small television camera tube that is used primarily in industrial television and studio film pickup because of its 600-line resolution, small size, simplicity, and spectral response approaching that of the human eye.

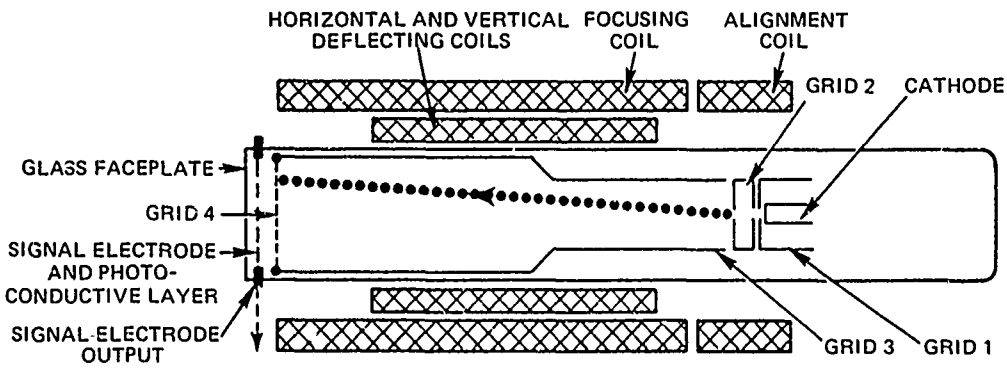

Fig. 17 VIDICON SCHEMATIC REPRESENTATION

As shown in Fig. 17, the tube consists of a signal electrode composed of a transparent conducting film on the inner surface of the faceplate; a thin layer (a few microns)

of photoconductive material deposited on the signal electrode; a fine mesh screen, grid 4, located adjacent to the photoconductive layer; a focusing electrode, grid 3, connected to grid 4; and an electron gun.

Principle of Operation

Each elemental area of the photoconductor can be likened to a leaky capacitor with one plate electrically connected to the signal electrode that is at some positive voltage (usually about 20 volts) with respect to the thermionic cathode of the electron gun and the other plate floating except when commutated by the electron beam. Initially, the gun side of the photoconductive surface is charged to cathode potential by the electron gun, thus leaving a charge on each elemental capacitor. During the frame time, these capacitors discharge in accordance with the value of their leakage resistance, which is determined by the amount of light falling on that elemental area. Hence, there appears on the gun side of the photoconductive surface a positive-potential pattern corresponding to the pattern of light from the scene imaged on the opposite surface of the layer. Even those areas that are dark discharge slightly, since the dark resistivity of the material is not infinite.

The electron beam is focused at the surface of the photoconductive layer by the combined action of the uniform magnetic field and the electrostatic field of grid 3. Grid 4 serves to provide a uniform decelerating field between itself and the photoconductive layer such that the electron beam always approaches the surface normally and at a low velocity. When the beam scans the surface, it deposits electrons where the potential of the elemental area is more positive than that of the electron-gun cathode and at this moment the electrical circuit is completed through the signal-electrode circuit to ground. The amount of signal current flowing at this moment depends upon the amount of discharge in the elemental capacitor, which in turn depends upon the amount of light falling on this area. The signal polarity is such that highlights in the scene swing the video-amplifier input negative.

Alignment of the beam is accomplished by a transverse magnetic field produced by external coils located at the base end of the focusing coil.

Deflection of the beam is accomplished by the transverse magnetic fields produced by external deflecting coils.

Vidicon Operating Considerations

The temperature of the faceplate of the tube should never exceed 60°C in either operation or storage. As the temperature increases, both the signal output current and the dark current (current that flows when the photoconductive surface receives no light) increase; however, the dark current increases faster and shading (unequalness of dark current at different points on the surface) in the output signal current becomes a serious problem. Further, as the signal-electrode voltage is increased, the signal output current-to-dark-current ratio decreases, thus increasing the shading problem.

Shielding of both the signal electrode and signal lead from external fields is highly important.

A blanking signal should be furnished to grid 1 or to the cathode to prevent the electron beam from striking the photoconductive surface during retrace of the horizontal and vertical sweeps.

Vidicon Signal and Noise

Since the vidicon acts as a constant-current generator as far as signal current is concerned, the value of the load resistor is determined by band-pass and noise considerations in the input circuit of the video amplifier. Where the signal current is less than 1 microampere and the band pass is relatively wide, the principal noise in the system is contributed by the input circuit and first stage of the video amplifier.

In addition to the standard vidicon mentioned above, there are a number of other more sophisticated types. One is the SILICON TARGET VIDICON which functions similar to the standard tube discussed above. The silicon target vidicon uses a matrix of silicon diodes in the target. This tube is approximately 100 times more sensitive and is not susceptible to solar damage. Other vidicon types are the SEC (Secondary Electron Conductivity) vidicon and the SIT (Silicon Intensifier Target) vidicon. Both of these tube types employ an imaging section in front of the vidicon target. In both cases the light signals are detected by a photoemissive thin-film semi-transparent photo-cathode. It is then an electron image rather than a photon image that impinges upon the vidicon target.

IMAGE ORTHICON

The image orthicon is a television camera tube having a sensitivity and spectral response approaching that of the eye. Commercially acceptable pictures can be obtained with incident illumination levels of 10 foot-candles.

As shown in Fig. 18, the tube comprises three sections: an image section, a scanning section, and a multiplier section.

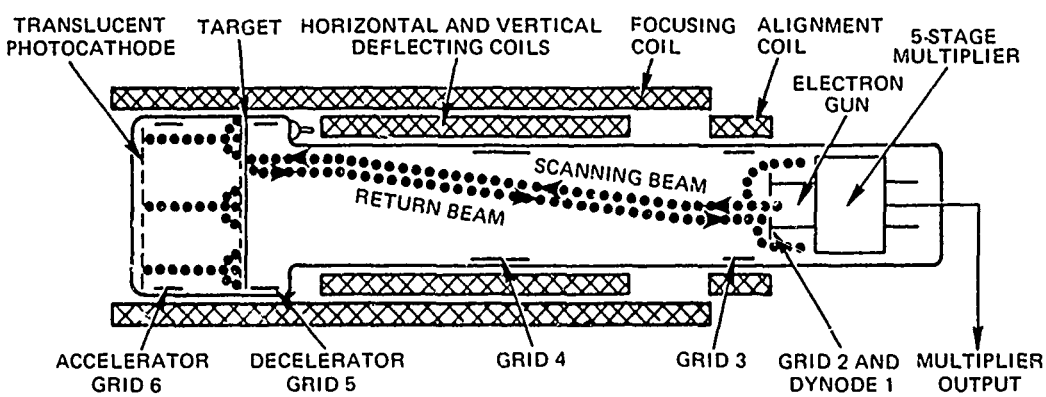

Fig. 18 IMAGE ORTHICON SCHEMATIC REPRESENTATION

Principle of Operation

From the light image focused on the photocathode, an electron image is derived that is accelerated to and magnetically focused in the plane of the target. These primary electrons striking the glass target (thickness of the order of a ten-thousandth of an inch and a lateral electrical resistivity of between 3×10^{11} and 10^{12} ohm-centimeter) cause the emission of secondary electrons that are collected by an adjacent mesh screen held at a small positive potential with respect to target-voltage cutoff. The photocathode side of the target thus has a pattern of positive charges that corresponds to the light pattern from the scene being televised; since the glass target is very thin, the charges set up a similar potential pattern on the opposite or scanned side of the glass.

In the scanning section, the target is scanned by a low-velocity electron beam produced by an electron gun. The beam is focused at the target by means of the axial magnetic field of the external focusing coil and the electrostatic field of grid 4. The decelerating field between grids 4 and 5 is shaped such that the electron beam always approaches normal to the plane of the target and is at a low velocity. If the elemental area on the target is positive, then electrons from the scanning beam deposit until the charge is neutralized; if the elemental area is at cathode potential (i.e., corresponding to the black picture area), no electrons are deposited. In both cases the excess beam electrons are turned back and focused into a 5-stage signal multiplier. The charges existing on either side of the target glass will conductively neutralize each other in less than one frame time. Electrons turned back at the target form a return beam that has been amplitude-modulated in accordance with the charge pattern of the target.

Alignment of the electron beam is accomplished by the transverse magnetic field of the external alignment coil. Deflection of the beam is produced by the transverse magnetic fields of the external horizontal and vertical deflecting coils.

In the multiplier section, the return beam is directed to the first stage of the electrostatically focused, 5-stage multiplier where secondary electrons are emitted in quantities greater than the striking primary electrons. Grid 3 facilitates a more complete collection by dynode 2 of the secondary electrons from dynode 1. The gain of the multiplier is high enough that the limiting noise in the use of the tube is the random noise of the electron beam rather than the input noise of the video amplifier.

Orthicon Operating Considerations

The temperature of the entire bulb should be held between 45 and 60°C since low target temperatures are characterized by a rapidly disappearing "sticking picture" of opposite polarity from the original when the picture is moved; high temperatures will cause loss of resolution and damage to the tube.

An overall potential of 1750V is necessary to operate the tube (+1250V at 1 mA, -500V at 1 mA, and -330V at 90 mA for the voltage divider and typical focusing and alignment coils).

Full-size scanning of the target should always be used during operation. The blanking signal, a series of negative-voltage pulses, should be supplied to the target to prevent the electron beam from striking the target during retrace. In the event of scanning failure, the beam must not reach the target.

It is necessary to add a shading-correction signal, of sawtooth shape and/or horizontal-scan frequency, to the video signal after it has been clamped to obtain a uniformly shaded picture.

SEE SAW* IMAGE CORRELATION TUBES

The ITT Industrial Laboratories announced the development and commercial availability of a new type of

* Trademark applied for.

electro-optical device, the See Saw image correlation tube. For added flexibility in various application requirements the See Saw image correlation tube is available in two different models. Type F4066 has a visual output presentation whereas Type F4067 provides an electrical output signal.

The See Saw image correlation tube is essentially a compact multi-channel computer, capable of automatically generating an output signal directly proportional to a cross-correlation integral between two consecutive input images. An even more important feature of the See Saw image correlation tube is that it has the ability of electronically deflecting one image across another image, generating a time-varying output signal exhibiting a clearly defined peak for the particular position of the two images for which maximum cross correlation exists.

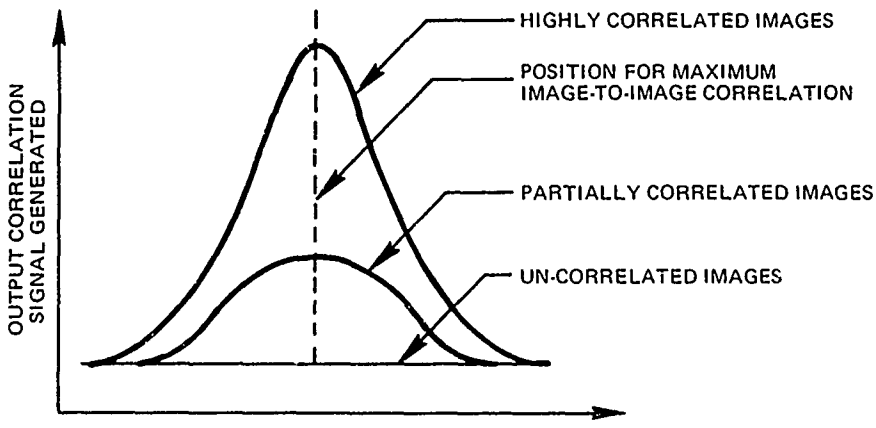

Fig. 19 SIGNAL CORRELATION OF TWO IMAGES

The key internal component of the See Saw image correlation tube is a composite storage mesh, similar to the meshes used in Iatron^R and other direct view storage tubes, consisting of metallic mesh upon which a thin insulating layer is deposited. The first of the two input images to be correlated is stored in the tube in terms of a charge

pattern, generated at the input photocathode, focused by a magnetic field, and deposited on the insulator layer. The operating potentials of the tube are then shifted electronically such that photoelectrons from the photocathode, generated by the second input optical image to be correlated, can no longer strike the insulator surface but are allowed to partially penetrate or reflect from the mesh holes, depending upon the magnitude of the stored charge pattern.

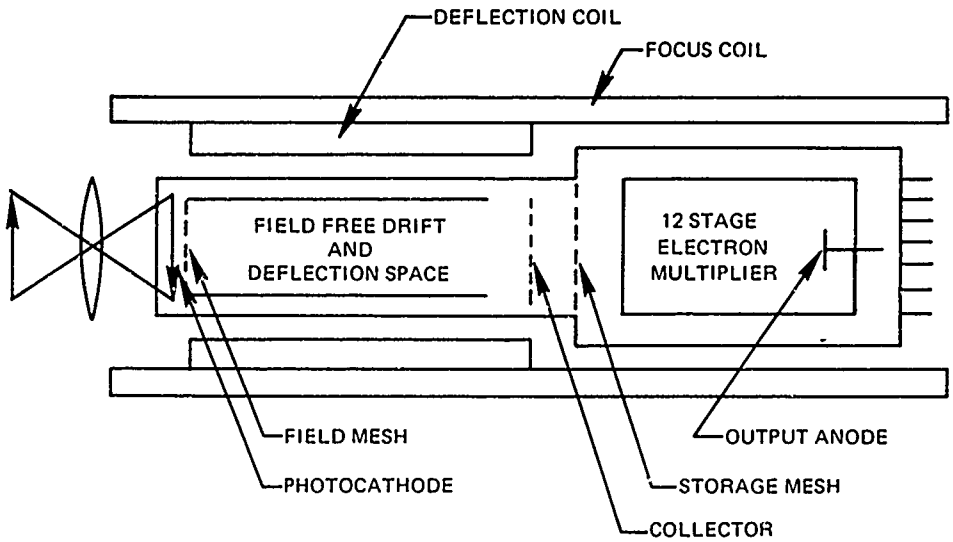

Fig. 20 TYPE F4067 SCHEMATIC

Since the charge pattern of the first image, $g(x, y, \theta, m)$ modulates the mesh transmission simultaneously on a point-by-point basis for the incident electron pattern, $j(x+\Delta x, y+\Delta y, \theta+\Delta\theta, m+\Delta m)$ of the second image, the tube directly generates the desired cross-correlation function image

$$\int g(x, y, \theta, m)\ j(x+\Delta x, y+\Delta y, \theta+\Delta\theta, m+\Delta m)\ dx\ dy\ d\theta\ dm$$

for each individual set of values of the relative image displacements, Δx, Δy, $\Delta\theta$, and Δm (θ and m are the image rotation and magnification respectively). Deflection coils are used to deflect the second image with respect to the first, generating a maximum correlation signal when maximum correlation exists.*

In many respects the See Saw image correlation tube is the closest technological approach yet to a substitute for the combination of human eye, optic nerve, and optical nerve center of the brain. It will undoubtedly enjoy widespread application for such pattern recognizing operations as map reading, V/H sensing, document reading, etc.

Figure 21 gives an outline drawing and preliminary specifications for the See Saw Correlation tubes, types F4066 and F4067.

---

*Image rotation and zoom are closely interrelated image manipulations achievable over limited ranges in the image correlation tube with appropriate non-uniform magnetic fields. Design of the required coils is, at present, left to the tube user.

Preliminary Specifications

(See Saw Image Correlation tubes, types F4066 and F4067)

General Characteristics:	F4066	F4067	Units
Photocathode type	S-20	S-20	
Wavelength of maximum response	4200	4200	Angstroms
Phosphor type	P-20	–	
Focus	Magnetic	Magnetic	
Deflection	Magnetic	Magnetic	
Typical Performance Characteristics: (for typical operating conditions)			
Threshold exposure	10^{-3}	10^{-3}	Fc · Sec
Number of resolvable elements	10^{5}	10^{5}	
Resolution (1000 line storage mesh)	20	20	line pairs/mm
Multiplier gain	–	10^{4}	
Photocathode luminous sensitivity	150	150	uA/lumen
Phosphor luminous efficiency	0.35	–	lumen/μA
Viewing screen brightness level	2	–	millilamberts
Typical Operating Conditions:			
Overall voltage		3	kV
Write-correlate voltage shift		500	Volt
Magnetic focus field		100-500	Gauss

Mechanical Data:

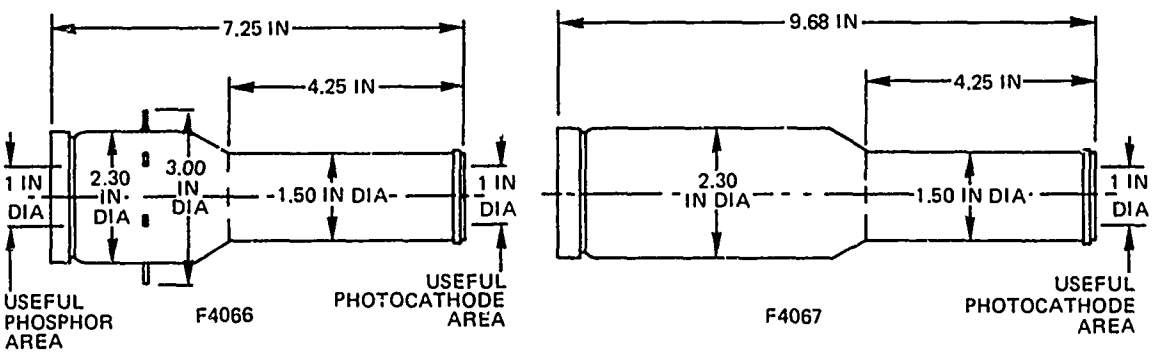

Fig. 21 CORRELATION TUBES OUTLINE DRAWINGS

6. STAR SENSOR SYSTEMS

A fair number of systems concepts are adequately described in the references given in the attendant listing. Mappers as well as trackers are described in detail.

Table 7 lists some of the factors influencing the frame rate for imaging type star sensor systems. Figure 22 gives a curve illustrating the false alarm probability as a function of sensor signal to noise ratio.

Table 7

Factors Influencing Image Frame Time

- Limitations imposed by mechanical mirror scan systems
- Libration rate of the satellite
- Input signal level to the detector
- Detector sensitivity
- Detector response time
- Desired spatial resolution
- Available transmitter RF power which has a direct bearing upon system bandwidth

Preceding page blank

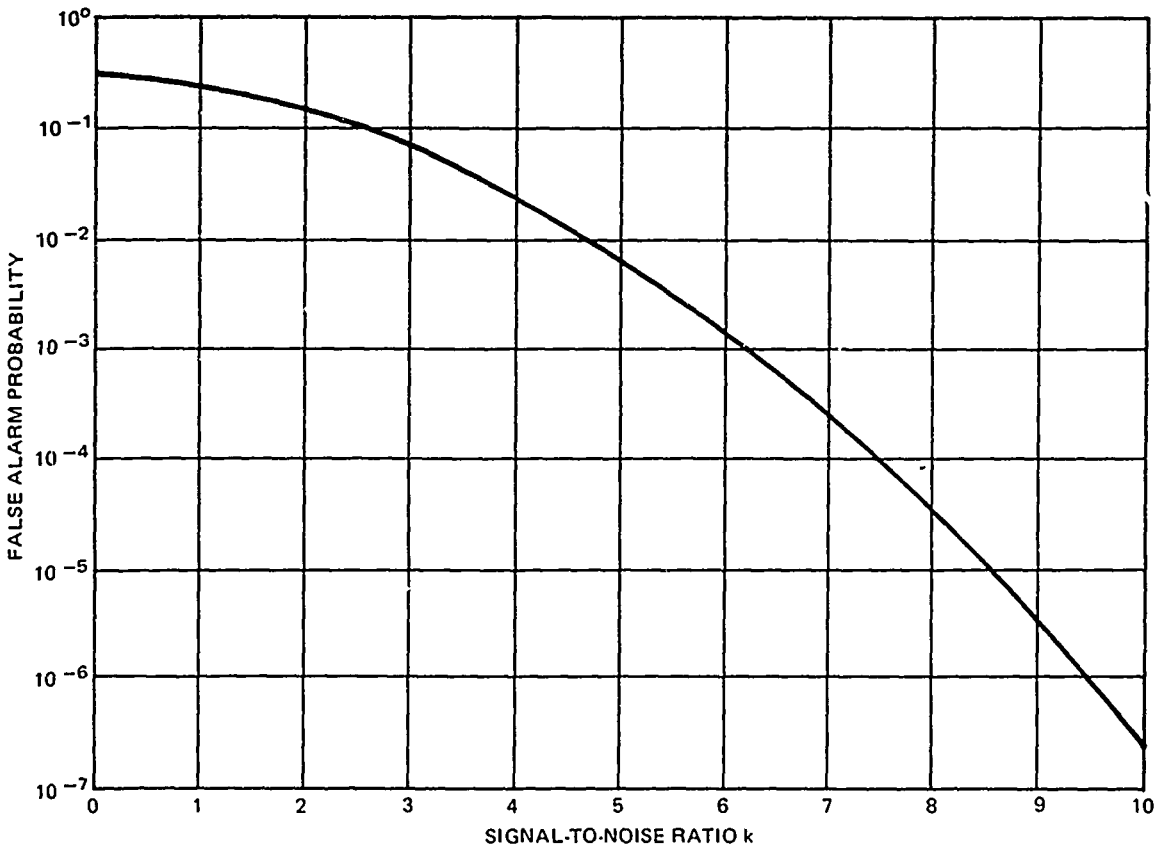

Fig. 22 THE RELATION BETWEEN FALSE ALARM PROBABILITY AND SIGNAL-TO-NOISE RATIO

7. REFERENCES

1. Quasius, Glenn, "A Topological Approach to the Analysis of Star Tracking Systems," IEEE Transactions on Aerospace and Navigational Electronics, September 1963.

2. NAQVI & Levy, "Some Astronomical and Geophysical Considerations for Space Navigation," IEEE Transactions on Aerospace and Navigational Electronics, September 1963.

3. Flink, J., "Star Identification by Optical Radiation Analysis," IEEE Transactions on Aerospace and Navigational Electronics, September 1963.

4. Federal Scientific Corporation, Experimental Verification of Star Identification by Optical Radiation Analysis, AD 614238 ASTIA.

5. McCanless, F. V., "A Systems Approach to Star Trackers," IEEE Transactions on Aerospace and Navigational Electronics, September 1963.

6. Abate, J. E., "Star Tracking and Scanning Systems, Their Performance and Parametric Design," IEEE Transactions on Aerospace and Navigational Electronics, September 1963.

7. Birnbaum, M., "The Astroguide – A Space Vehicle Navigation System," IRE International Conv., March 1962 in New York City or from Librescope Division General Precision, Inc., Glendale, California.

8. Zito and Malkiel, "Design Criteria of the Bendix Multipurpose Star and Planet Tracker," Intl. Aerospace Instrumentation Symposium, March 1966, Cranfield, Bedford, England or from Eclipse Pioneer Division, The Bendix Corporation, Teterboro, New Jersey.

9. The Jet Propulsion Laboratory, "The Canopus Tracker," pp. 46 to 51 of PL Space Programs Summary No. 37-29, Vol. II, May 1963 and pp. 25 to 37 of No. 37-29, Vol. II, September 1964.

10. Atwill, W., "Star Tracker Uses Electronic Scanning," Electronics, September 30, 1960.

11. Zuckerbraun, J., "Advanced Star Tracking Techniques," Kollsman Instrument Corp., AD 311389, ASTIA.

12. Honeywell, Aeronautical Division, Analysis of the Application of Image Forming Photosensors to Wide Field-of-View Daylight Star Trackers, N65-10849, NASA Scientific and Technical Information Facility or AD 604589, ASTIA.

13. Ceckowski and Polye, "Bendix Star Tracker Photomultiplier Tube," IEEE International Record, 1964, pp. 25-33.

14. Papp, G., "Limits of Resolution in Magnetically Focused Image Converter Tubes," ITT Federal Labs, Ft. Wayne, Indiana.

15. Eberhardt, E., "Accuracy of Position Determination in Star Tracker Tubes," IEEE Transactions on Aerospace Support Conference Procedures or ITT Industrial Labs.

16. Chapman, D., "Signal to Noise Power Ratio Available from Photomultiplier used as Star Detector in Star Tracking Systems," Journal British IRE, March 1962.

17. Shigemoto and Dishman, Image Dissector Aperture Geometrics and Scan Patterns for Use in Star Tracker Systems, NASA Technical Note TN D-2990 available from NASA Scientific and Technical Information Facility, # N-65-32399.

18. Leudicke, Cope and Flory, "Astronomical Image Integration System using a Television Camera Tube," Journal of Applied Optics, pp. 677-689, June 1964.

19. Zuckerbraun, J., "High Reliability Scanner for Stellar Navigation," Electronics, pp. 82-85, May 11, 1962.

20. Laverty, N. P., "The Comparative Performance of Electron Tube Photodetectors in Terrestrial and Space Navigation Systems," IEEE Transactions on Aerospace and Navigational Electronics, September 1963.

21. Nortronics Division, Northrop Corp., Validation of the Vidicon as a Detector for Advanced Celestial Equipment, AD 344509, ASTIA.

22. ITT, "Characteristics of Image Forming Tubes," Reference Data for Radio Engineers, 5th Edition, 1969.

23. ITT Research Memo E-6, "The Unique Properties of the Image Dissector," 1963.

24. Andren, C. F. and Schenkel, F. W., A Star Tracker Design for Synchronous Altitude Satellites, APL/JHU TG 869, November 1966.

25. Schenkel, F. W., Photometric and Optical Considerations in the DODGE Satellite TV Camera Design, APL/JHU Technical Digest, May-June 1967.

26. Schenkel, F. W. and Finkel, A., Star Sensor/Mapper with a Self-Deployable, High Attenuation Light Shade for SAS-B, APL/JHU CP-017, July 1972.

27. Beal, R. C., Photoelectric Imaging Devices for Astronomy, APL/JHU TG 1011, July 1968.

28. Allen, C. W., Astrophysical Quantities, Althone Press, University of London, England, 1955.

29. Handbook of Geophysics for Air Force Designers, USAF Cambridge Research Center, ch. 16, 1957.

30. Moon, P., "Proposed Standard Solar-Radiation Curves for Engineering Use," J. Franklin Inst., 1940.

31. Mahan, A. I., "Astronomical Refraction – Some History and Theories," Journal of Applied Optics, pp. 497-511, July 1962.

32. Ellison, M. H., "The Effects of Scintillation of Telescopic Images," Proc. Symp. on Astronomical Optics, North Holland Publishing Co., Amsterdam, The Netherlands, 1956.

33. Hosfeld, R., "Comparisons of Stellar Scintillations with Image Motion," J.O.S.A., Vol. 44, p. 284, 1954.

34. Furth, R., "Statistical Analysis of Scintillations of Stars," Proc. Symp. on Astronomical Optics, North Holland Publishing Co., Amsterdam, The Netherlands, 1956.

35, Brown, D. C., A Treatment of Analytical Photogrammetry with Emphasis on Ballistic Camera Applications, ASTIA Doc. No. 124144 (AF MTC Test Rept. 57-22).

36. Nagel, M. R., Geophysics Research Notes, Air Force Cambridge Research Center, Bedford, Mass., No. 46, November 1960.

37. American Institute of Physics Handbook, McGraw-Hill Book Co., Inc., New York, N. Y., 1957.

38. Kuiper, G. P. (Ed.), The Earth as a Planet, The University of Chicago Press, Chicago, Ill.

39. Roach, F. E. and Megill, L. R., "Integrated Starlight over the Sky," Astrophys. J., Vol. 133, pp. 228-242, January 1961.

40. Chamberlain, J. W., "Aurora and Airglow," Astronautics, August 1962.

41. Rosenberg, N. W., Hamilton, W., and Lovell, D. J., "Rocket Exhaust Radiation Measurements in the Upper Atmosphere," Journal of Applied Optics, Vol. 1, pp. 115-120, March 1962.

42. Ross, J. R., An Investigation of Missile Bloom, Radiation, Inc., Melbourne, Fla., Air Force Cambridge Research Labs Rept. 62-271, Contr. No. AF19-604-7980, February 1962.

43. Becvar, A., Skalnate Pleso Atlas of the Heavens, Sky Publishing Corp., Cambridge, Mass.

44. Friedman, H., "IGY Solar Flare Program and Ionizing Radiation in the Night Sky," Am. Rocket Soc. J., Vol. 29, pp. 103-107, February 1959.

45. Ramsey, R. C., "Spectral Irradiance from Stars and Planets above the Atmosphere from 0.1 to 100 microns," Appl. Opt., Vol. 1, pp. 465-471, July 1962.

46. Baker, C. B., and Petersen, M., Photo-Electric Stellar Magnitudes of Stars Brighter than 4.0 Magnitude, E-845 M.I.T. Instrumentation Lab., Cambridge, Mass., July 1959.

47. Johnson, F. S., "Atmospheric Structure," Astronautics, Vol. 7, August 1962.

48. Black, H. S., Modulation Theory, D. Van Nostrand Co., Inc., Princeton, N. J., 1953.

49. Schwartz, M., Information Transmission, Modulation and Noise, McGraw-Hill Book Co., Inc., New York, N. Y., 1959.

50. Bennett, W. R., "Methods of Solving Noise Problems," Proc. IRE, Vol. 44, pp. 609-638, May 1956.

51. Sandeman, E. K., "FM Star-Lock Systems using Mask with Linear Sector," IRE Trans. on Aerospace and Navigational Electronics, Vol. ANE-9, pp. 24-34, March 1962.

52. Mengers, P. E., Tracking Accuracy of Infrared Trackers, General Electric Co., Rept. No. R59ELC100, January 1960.

53. Smith, M. A., "The Relative Advantages of Coherent and Incoherent Detectors; a Study of their Output Noise Spectra under Various Conditions," Proc. IRE, No. 6, August 1956.

54. Middleton, D., "Rectification of a Sinusoidally Modulated Carrier in the Presence of Noise," Proc. IRE, Vol. 37, pp. 1467-1477, December 1948.

55. Tuller, W. G., "Theoretical Limitations on the Rate of Transmission of Information," Proc. IRE, Vol. 36, pp. 468-478, May 1949.

56. Jones, R. C., "Quantum Efficiency of Detectors for Visible and Infrared Radiation," in Advances in Electronics and Electron Physics, L. Marton (Ed.), Academic Press, Inc., New York, N. Y., Vol. 11, pp. 88-183, 1959.

57. Star Tracker Aerospace Reference Study, Aeronautical Sys. Div., Air Force Syst. Command, Minneapolis-Honeywell Regulator Co., Aeronautical Div., St. Petersburg, Fla., Tech Data Rept. 62-1056, 1963.

58. Slater, J. M., Stars in Ecliptic Coordinates, North American Aviation Pub. P5-1051/32, April 1965.

59. Slater, J. M., Daylight Star Tracking, North American Aviation Pub. P4-909/32, February 1965.

60. Norton's Star Atlas and Reference Handbook, Sky Publishing Corporation, Cambridge, Mass., 1973.

INITIAL DISTRIBUTION EXTERNAL TO THE APPLIED PHYSICS LABORATORY*

The work reported in TG 1256 was done under Navy Contract N00017-72-C-4401. This work is related to Task ID30 which is supported by NASA.

ORGANIZATION	LOCATION	ATTENTION	No. of Copies
DEPARTMENT OF DEFENSE			
DDC	Alexandria, Va.		12
Department of the Navy			
NAVSEASYSCOM	Washington, D. C.	SEA-09G3	2
NAVAIRSYSCOM	Washington, D. C.	AIR-50174	2
Navy Space Projects Office	Washington, D. C.	PM-16-22	1
NAVPRO	Silver Spring, Md.		1
Facilities			
NavAstroGru	Ft. Mugu, Calif.	CO	1
Navy Space Systems Activity	Los Angeles, Calif.	CO	1
Naval Observatory	Washington, D. C.	Dir., Time Service Div.	1
Laboratories			
NOL	White Oak, Md.	Tech. Library	1
Department of the Air Force			
Centers			
DMA, Aerospace Ctr.	St. Louis, Mo.	PDEG	1
Commands			
Air University	Maxwell AFB, Ala.	Tech. Library	1
U.S. GOVERNMENT AGENCIES			
National Aero. and Space Admin.			
Hq., Office of Space Sciences	Washington, D. C.	M. J. Aucremanne (Code SG)	4
NASA Scientific and Technical Information Facility	College Park, Md.	J. Waldo	1
Goddard Space Flight Ctr.	Greenbelt, Md.	Library - 252	1
		Mrs. M. R. Townsend	1

Requests for copies of this report from DoD activities and contractors should be directed to DDC, Cameron Station, Alexandria, Virginia 22314 using DDC Form 1 and, if necessary, DDC Form 55.

*Initial distribution of this document within the Applied Physics Laboratory has been made in accordance with a list on file in the APL Technical Publications Group.